The extracellular matrix of human bone marrow adipocytes and glucose concentration differentially alter mineralization quality without impairing osteoblastogenesis

Laura Entz, Guillaume Falgayrac, Christophe Chauveau, Gilles Pasquier, Stéphanie Lucas

Bone Reports 17 (2022) 101622

Contents lists available at ScienceDirect

Bone Reports

journal homepage: www.elsevier.com/locate/bonr

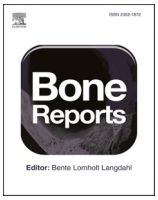

The extracellular matrix of human bone marrow adipocytes and glucose concentration differentially alter mineralization quality without impairing osteoblastogenesis

Laura Entz, Guillaume Falgayrac, Christophe Chauveau, Gilles Pasquier, Stéphanie Lucas *

Marrow Adiposity and Bone Lab, MABLab-ULR4490, Univ. Littoral Côte d'Opale F-62200 Boulogne-sur-Mer, Univ. Lille F-59000 Lille, CHU Lille, F-59000 Lille, France

ARTICLE INFO

Keywords:
Marrow adipocytes
Extracellular matrix
Skeletal mesenchymal stromal cells
Osteoblast
Hyperglycemia
Osteoporosis

ABSTRACT

Bone marrow adipocytes (BMAds) accrue in various states of osteoporosis and interfere with bone remodeling through the secretion of various factors. However, involvement of the extracellular matrix (ECM) produced by BMAds in the impairment of bone marrow mesenchymal stromal cell (BM-MSC) osteoblastogenesis has received little attention. In type 2 diabetes (T2D), skeletal fragility is associated with several changes in bone quality that are incompletely understood, and BMAd quantity increases in relationship to poor glycemic control. Considering their altered phenotype in this pathophysiological context, we aimed to determine the contribution of the ECM of mature BMAds to osteoblastogenesis and mineralization quality in the context of chronic hyperglycemia.

Human BM-MSCs were differentiated for 21 days in adipogenic medium containing either a normoglycemic (LG, 5.5 mM) or a high glucose concentration (HG, 25 mM). The ECM laid down by BMAds were devitalized through cell removal to examine their impact on the proliferation and differentiation of BM-MSCs toward osteoblastogenesis in LG and HG conditions. Compared to control plates, both adipocyte ECMs promoted cell adhesion and proliferation. As shown by the unmodified RUNX2 and osteocalcin mRNA levels, BM-MSC commitment in osteoblastogenesis was hampered by neither the hyperglycemic condition nor the adipocyte matrices. However, adipocyte ECMs or HG condition altered the mineralization phase with perturbed expression levels of type 1 collagen, MGP and osteopontin. Despite higher ALP activity, mineralization levels per cell were decreased for osteoblasts grown on adipocyte ECMs compared to controls. Raman spectrometry revealed that culturing on adipocyte matrices specifically prevents type-B carbonate substitution and favors collagen cross-linking, in contrast to exposure to HG concentration alone. Moreover, the mineral to organic ratio was disrupted according to the presence of adipocyte ECM and the glucose concentration used for adipocyte or osteoblast culture. HG concentration and adipocyte ECM lead to different defects in mineralization quality, recapitulating contradictory changes reported in T2D osteoporosis.

Our study shows that ECMs from BMAds do not impair osteoblastogenesis but alter both the quantity and quality of mineralization partly in a glucose concentration-dependent manner. This finding sheds light on the involvement of BMAds, which should be considered in the compromised bone quality of T2D and osteoporosis patients more generally.

1. Introduction

Bone marrow adipocytes (BMAds) have been revealed as important contributor cells in bone homeostasis. These lipid-laden cells primarily arise in close vicinity of trabeculae within the long bones or vertebrae and dramatically accrue in various types of osteoporosis, such as due to aging, menopause, and type 2 diabetes (T2D) (Hardouin et al., 2016). The bone marrow (BM) fat fraction negatively correlates with bone

Abbreviations: AGEs, Advanced glycation end-products; BMAd, Bone marrow adipocyte; BM-MSC, Bone marrow mesenchymal stromal cell; ECM, Extracellular matrix; ECM_{BMAd}, Extracellular matrix obtained from BMAds; ECM_{BMAd} LG, Extracellular matrix obtained from BMAds cultured in LG concentration; ECM_{BMAd} HG, Extracellular matrix obtained from BMAds cultured in HG concentration; GAG, glycosaminoglycan; HA, hydroxyapatite; HG, High glucose; LG, Low glucose; LGM, Low glucose and mannitol; T2D, Type 2 diabetes.

* Corresponding author.
E-mail address: stephanie.lucas@univ-littoral.fr (S. Lucas).

https://doi.org/10.1016/j.bonr.2022.101622
Received 25 July 2022; Received in revised form 9 September 2022; Accepted 19 September 2022
Available online 20 September 2022

mineral density (BMD) in aging and menopause. It is also strongly associated with poor glycemic control in T2D (Andrade et al., 2021; Yu et al., 2017), which is characterized by unchanged or even increased bone mass with compromised bone quality (Schwartz, 2016). While BMAds can potentially affect both bone quantity and quality, their role has been primarily investigated in relation to bone remodeling. Bone marrow mesenchymal stromal cells (BM-MSCs) are considered a common precursor for BMAds and osteoblasts, and their preferential diversion toward the adipocyte lineage has been reported to reduce bone formation (Sadie-Van Gijsen et al., 2013). BMAds can also modulate osteoblastogenesis and stimulate osteoclastogenesis through paracrine factors (Hardouin et al., 2016; Rharass and Lucas, 2018; Wang et al., 2021). To date, the involvement of the extracellular matrix (ECM) produced by BMAds has not been thoroughly examined (Craft and Scheller, 2016).

The ECM, through its proper components as well as its capacity to bind and release factors, is well known to create a biochemical and a physical environment that interacts with cells to modify their behavior. *In vitro* cell-free ECMs (obtained through various devitalization processes) have been shown to drive these changes more efficiently than a precoating of key ECM components (Lai et al., 2010). The ECMs generated by either BM-MSCs (Chen et al., 2007; Lai et al., 2010) or osteoblasts (Baroncelli et al., 2018b; Hoshiba et al., 2009; Li et al., 2019) improve BM-MSC proliferation, osteogenic differentiation and mineralization. Studies of the impact of adipocyte ECM on these functions are currently limited. The ECM produced by adipocytes during the early stage of differentiation from either human BM-MSCs (Hoshiba et al., 2010, 2012) or extramedullary adipose tissue stem cells (Guneta et al., 2017) favors the commitment toward adipogenesis rather than osteoblastogenesis. Devitalized ECM composition reflects cell specificity (Guneta et al., 2017; Hoshiba et al., 2009, 2010), but the microenvironment and its afferent signaling cues also modify its components and consecutively influence cell fate (Sun et al., 2011) and activity (Baroncelli et al., 2018b). Because BMAds activities adapt according to the pathophysiological context (Hardouin et al., 2016; Tencerova et al., 2021), the marked development of adipocytes in the BM could alter the balance between adipogenesis and osteoblastogenesis by the synthesis of a specific ECM.

A decline in glucose homeostasis is often associated with aging and menopause, while chronic hyperglycemia is the hallmark of T2D. In these osteoporotic contexts, bone quality can vary independently of BMD, more specifically in T2D, contributing to an increased risk of fracture (Boskey and Imbert, 2017; Lekkala et al., 2019). The assessment of bone quality encompasses several aspects and primarily includes characterization of the organic and mineral components of bone. These measurements have been considerably upgraded using vibrational spectroscopic techniques with spatial resolution (Boskey and Imbert, 2017; Gamsjaeger et al., 2014). Combined with the analyses of mechanical tests in animal models or fracture history in patients, several parameters, such as collagen maturity, extent of mineralization, mineral stoichiometry, or carbonate substitution of the apatite crystal, have been shown to contribute to bone strength (Boskey and Imbert, 2017; Gamsjaeger et al., 2014; Lekkala et al., 2019). In the T2D context, the accumulation of advanced glycation end-products (AGEs) in the protein matrix is considered to be driven by high glucose (HG) levels and oxidative stress and to interfere with bone properties (Karim et al., 2019; Lekkala et al., 2019; Moseley et al., 2021). However, several studies have qualified the importance of AGEs in bringing attention to a large array of other bone quality components (Creecy et al., 2018; Hunt et al., 2018, 2021; Karim et al., 2018). The study of the direct impact of HG concentration on osteoblast mineralization was undertaken early *in vitro* to show divergent defects in cellular calcium accumulation and a modified calcium to phosphorus ratio in the mineral (Balint et al., 2001; García-Hernández et al., 2012). Indeed, greater attention has been given to the effects of HG concentration on proliferation (Hankamolsiri et al., 2016; Keats and Khan, 2012; Shao et al., 2014; Wang et al., 2010; Zhang and Yang, 2013) and the differentiation potential of various precursor types. Following a relatively short-term culture, HG concentrations have been reported to promote adipogenesis over osteoblastogenesis in human BM-MSCs (Hankamolsiri et al., 2016; Keats and Khan, 2012) and rodent bone marrow stromal cells (Chaves Neto et al., 2018; Chuang et al., 2007; Wang et al., 2014). Moreover, *in vivo* experiments (Suchacki et al., 2020), *ex vivo* characterization of BMAds from T2D patients (Ferland-McCollough et al., 2018) and *in vitro* studies (Keats and Khan, 2012; Keats et al., 2014; Rharass and Lucas, 2019) support that BMAds are responsive to glucose levels and adapt their phenotype accordingly. Specifically, our group showed *in vitro* that mature human BMAds produce more intracellular and extracellular reactive oxygen species (ROS) when exposed to an HG concentration (Rharass and Lucas, 2019), indicating that BMAds could damage bone quality in the context of uncontrolled hyperglycemia.

Considering the accrual of BMAds and their altered phenotype in the T2D pathophysiological context, the aim of this study was to assess whether the ECM provided by mature human BMAds in an HG concentration interferes with osteoblastogenesis and mineralization quality. Human BM-MSCs were differentiated and matured in adipogenic medium containing either a normoglycemic glucose concentration (LG) or an HG concentration. The ECMs laid down by BMAds were thus devitalized to determine their impact on proliferation and differentiation toward osteoblastogenesis of BM-MSCs. Considering the effect of HG on BM-MSC differentiation, osteoblastogenesis was also studied under LG and HG conditions on the two types of adipocyte ECMs using classical culture plates as a control. The different osteoblast cultures were characterized through gene expression and functional assays, while the quality of mineralization was measured using Raman spectroscopy.

2. Materials and methods

2.1. Culture of human BM-MSCs and differentiation toward adipogenesis

Prescreened human BM-MSCs obtained from RoosterBio were cultured using Dulbecco's modified Eagle's medium (DMEM) supplemented with 10 % fetal bovine serum (FBS), 1 % L-glutamine, 1 % penicillin/streptomycin (all from PanBiotech) and 5.5 mM glucose at a density of 1.1×10^4 cells/cm^2 up to 80 % cell confluence followed by subsequent passages (cell proliferation) or differentiation. All cultures were incubated at 37 °C and 5 % CO_2 in a humidified atmosphere. All experiments were performed between passages 4 and 5 using four donors (2 females, 20 and 26 years, and 2 males, both 25 years).

Human BM-MSCs were seeded at a density of 1.1×10^4 cells/cm^2 and differentiated into BMAds using complete DMEM (with FBS, L-glutamine and penicillin/streptomycin) containing either LG (5.5 mM to represent normal glycemia) or HG concentration (25 mM to mimic severe diabetes) supplemented with 6.25 µg/mL insulin (PanBiotech), 0.5 µM dexamethasone, 0.5 mM 3-isobutyl-1-methylxanthine and 50 µM indomethacin (all from Sigma). Adipogenic media were replaced every 3–4 days for up to 21 days of culture. This step corresponds to the Fig. 1A of the experimental design.

2.2. Preparation of decellularized ECM from BMAds and quality assessment

After 21 days in adipogenic media, mature BMAds generated in either LG or HG concentrations were washed twice in Dulbecco's phosphate buffered saline (DPBS, no calcium, no magnesium - Dutscher), and devitalization was performed by hypotonic shock adapted from previous studies (Rossi et al., 2018; Wang et al., 2013). Demineralized sterile water at room temperature was gently added to the cells and removed after 7 mins of incubation. This step was then repeated 5 times in a row. The remaining components were washed twice in DPBS and incubated for 30 min at 37 °C in a sterile solution of lipase (40 U/L, Sigma) and DNase (10 U/mL, Roche). After confirmation of complete cell lysis by

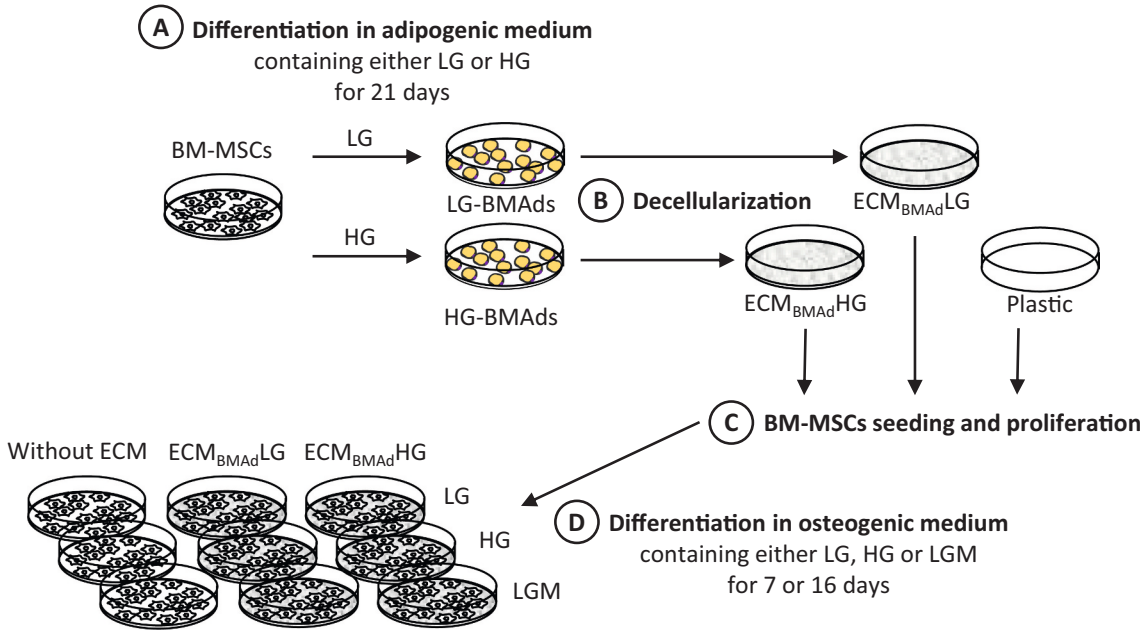

Fig. 1. The four stages of the experimental plan
(A) Human BM-MSCs were differentiated into BMAds for 21 days in adipogenic medium containing either 5.5 (LG) or 25 mM glucose (HG). (B) The two types of BMAds were devitalized to obtain their respective ECMs, referred to as ECM_{BMAd}LG and ECM_{BMAd}HG. (C) BM-MSCs were seeded on ECM_{BMAd}LG, ECM_{BMAd}HG or on plastic ("without ECM" as a control) to study adhesion and proliferation under LG condition. (D) Using the three types of support and after 48 h of seeding, BM-MSCs were differentiated into osteoblasts for 7 or 16 days in osteogenic medium containing either 5.5 mM (LG) or 25 mM (HG) glucose or 5.5 mM glucose +20 mM mannitol (LGM) to analyze several parameters related to osteoblastogenesis and mineralization.

microscopic observation, the resulting devitalized ECMs, referred to as ECM_{BMAd} LG or ECM_{BMAd} HG, were gently washed twice with DPBS, air dried and frozen at −80 °C until use (Fig. 1B).

Decellularization was confirmed by the absence of nuclear materials and cellular components such as lipid droplets. Following fixation in 2 % paraformaldehyde, washing steps with DPBS and then labeling with DAPI (1,2 μg/mL) and BODIPY (1:200) (both from Invitrogen) in DPBS for 30 mins, plates were visualized using an Axioskop50 Fluorescence Microscope (Carl Zeiss), and images were acquired using Histolab software (Microvision Instrument). Protein measurements were performed using DC Protein assay (Bio-Rad) and a BSA standard curve.

For each subsequent experiment, human BM-MSCs from a donor were seeded on the corresponding ECM_{BMAd} produced by this same donor.

2.3. Attachment, proliferation, and characterization of human BM-MSCs on decellularized ECM_{BMAd}

Human BM-MSCs from each donor were seeded at a density of 8.3 × 10^3 cells/cm^2 on the corresponding decellularized matrices (ECM_{BMAd} LG or ECM_{BMAd} HG) or on plastic (control referred to as without ECM) and cultured in complete DMEM with 5.5 mM glucose. DNA level was quantified at 24, 48 and 96 h after seeding using the CyQUANT Cell Proliferation Assay Kit (Invitrogen) according to the manufacturer's instructions. The DNA-bound fluorescence was measured using a Xenius XMA fluorescence microplate reader (SAFAS) at ~500 nm excitation and ~530 nm emission maxima in each lysed sample. The parameter settings were kept constant for all comparative sets of experiments. Finally, the amount of DNA was calculated from a standard curve and converted to the number of cells (one cell corresponding to 242 pg DNA).

For characterization, BM-MSCs were collected after 1 and 2 days in LG complete medium in Extract-All (Eurobio) for RNA extraction (Fig. 1C).

2.4. Human BM-MSC differentiation into osteoblasts on decellularized ECM_{BMAd}

Human BM-MSCs were seeded at a density of 8.3 × 10^3 cells/cm^2 on decellularized ECM_{BMAd} LG, ECM_{BMAd} HG or on plastic (without ECM) and cultured in complete DMEM with 5.5 mM glucose. After 2 days (~60 % confluence), human BM-MSCs were differentiated into osteoblasts using complete DMEM containing either 5.5 mM glucose (LG), 25 mM glucose (HG) or 5.5 mM glucose and 20 mM mannitol (denoted as LGM; to address the osmolarity effect of HG). All osteogenic media were supplemented with 10 μM β-glycerophosphate, 50 μM ascorbic acid, 0.1 μM vitamin D3 and 10 nM dexamethasone (all from Sigma) and were replaced every 3–4 days up to 7 and 16 days of culture for the specified experiments (Fig. 1D).

2.5. RNA extraction, reverse transcription and RT–PCR analysis

Total RNAs were extracted using Extract-All following the manufacturer's instructions. Residual contaminating genomic DNA was digested with 2.5 U/μl DNase I recombinant (Roche). Reverse transcription was performed from 250 ng of RNA using a Maxima First Strand cDNA Synthesis Kit (Thermo Scientific). Real-time PCR was performed using PowerUp SYBR Green Master Mix (Applied Biosystems) using StepOne Real-Time PCR System (Applied Biosystems). Primers were designed using OLIGO Primer Analysis Software 6 (Molecular Biology Insights) and used when efficiency was >1.8. The primers used are listed in Supplemental Table 1. Amplifications were performed according to the manufacturer's instructions. A melting curve analysis confirmed product specificity. The relative mRNA expression of the tested genes was calculated according to Ct values and primer efficiencies (E) and then normalized to those calculated for the ribosomal protein L13a (*RPL13A*) housekeeping gene according to $E_{gene}^{-Ctgene}/E_{ref}^{-Ctref}$. As indicated for each figure, relative mRNA expression levels were appropriately normalized as the fold level according to the considered control of the experiment.

2.6. Protein extraction and western blot analysis

After 16 days, osteogenic media were removed before PBS washing and scraping of cells and mineralized nodules in cold RIPA buffer supplemented with a final concentration of 2 % SDS, 1 % deoxycholate sodium and 2× protease inhibitors (Pierce). Total proteins were extracted at 4 °C using 30 min of vortexing and sonication. Following protein concentration determination as stated in section 2.2, 20 μg of proteins per sample were labeled with Cy5 dye (Amersham QuickStain Protein Labeling kit) according to the manufacturer's instructions and separated using 8 % SDS–PAGE. Following blotting on nitrocellulose in methanol, Cy5-labeled proteins were detected using the Amersham Imager 600 (GE Healthcare). After blocking in TBST with 5 % nonfat dry milk, the membrane was incubated overnight at 4 °C with a monoclonal rabbit antibody against type I collagen (Ab138492, diluted 1:1000, Abcam) in TBST with 1 % milk. Following washing steps and incubation with the secondary anti-rabbit HRP antibody (at 1/15000th, STAR124P, BioRad), imaging of type I collagen protein (COLI) was acquired using ECL Prime (Amersham). The signal intensities of Cy-5-labeled proteins and COLI were measured using Image Quant TL analysis software (Amersham) to express the quantity of COLI according to the amount of total loaded and blotted proteins (*i.e.*, sum of the intensities of Cy-5-labeled proteins).

2.7. Alkaline phosphatase (ALP) activity measurement

After 16 days in osteogenic media, the cells were rinsed with DPBS and frozen at −80 °C until further use. After thawing, the cells were harvested in 0.2 % Nonidet P-40, sonicated for 30 s and then centrifuged to collect only the supernatant.

To determine ALP activity, 10 μL of sample was mixed with 90 μL of a solution containing 10 nM *p*-nitrophenyl phosphate, 0,56 M 2-amino-2-methyl-1-propanol (pH 10,3) and 1 mM $MgCl_2$. After 4 min at 37 °C, the reaction was stopped by the addition of 40 μL of 1 M NaOH, and the absorbance was measured at 405 nm. Values were expressed according to the protein content in each sample as measured by DC Protein assay (Bio-Rad). Finally, ALP activity was determined according to the following calculation: (Absorbance × 1000)/(18.182 × minutes of incubation × volume of sample)/protein concentration.

2.8. Measurement of cell mineralization by fluorescent hydroxyapatite staining

After 16 days in osteogenic media, cells were fixed in 2 % paraformaldehyde, rinsed three times, and then stained with the Osteoimage Mineralization Assay (Lonza) in the dark for 30 mins according to the manufacturer's instructions. After washing, fluorescence was measured using a Xenius XC spectrofluorometer (SAFAS) at 492 and 500 nm (excitation and emission, respectively). Following cell number determination using the CyQUANT Cell Proliferation Assay Kit, the cell mineralization level was expressed by calculating the fluorescence value-to-cell number ratio.

2.9. Raman spectroscopy

Human BM-MSCs were seeded at 1.1×10^4 cells/cm^2 on Raman grade CaF_2 slides (dimension 13 × 1 mm, Crystran) and differentiated into BMAds using adipogenic media containing either LG or HG as described in Section 2.1. After 21 days, the cells were fixed (2 % paraformaldehyde) or decellularized (as described in Section 2.2) prior to fixation to validate the decellularization and the integrity of the ECM after the devitalization process. Moreover, CaF_2 slides without ECM or with ECM_{BMAd} were used to seed and culture human BM-MSCs (cell density of 8.3×10^3 cells/cm^2 for seeding) in osteogenic media (Section 2.4) for 16 days. Osteoblasts were fixed in 2 % paraformaldehyde to measure mineralization parameters.

After rinsing, the fixed samples were analyzed using a LabRAM HR800 microspectrometer (HORIBA; Jobin Yvon, Villeneuve d'Ascq, France). The Raman analysis was performed using a diode laser (λ = 785 nm) and an immersive Nikon water objective (×100, NA = 1.25). The acquisition time was set to 30 s and averaged 2 times. From the different Raman spectra, the amount of glycosaminoglycans (GAGs) contained in each ECM_{BMAd} was quantified as the area ratio of the bands at 1318 and 1338 cm^{-1} (Mainreck et al., 2011) over the phenylalanine area. Regarding the mineralized nodules laid down by osteoblasts, the following physicochemical parameters were evaluated: 1) collagen crosslinks as the intensity ratio of the bands 1660 cm^{-1} with 1690 cm^{-1} is also referred to as collagen maturity (Boskey and Imbert, 2017; Gamsjaeger et al., 2017); 2) pyridinoline trivalent crosslinks as the ratio of the intensity 1660 cm^{-1} over the amide I area (Gamsjaeger et al., 2017); 3) mineral/organic ratio defined as the ratio of the band area 960 cm^{-1} (ν_1PO_4) over 1002 cm^{-1} (phenylalanine), which corresponds to the relative amount of mineral over organic amount; 4) type-B carbonate substitution defined as the ratio of band area of 1070 cm^{-1} (ν_1CO_3) over band area 960 cm^{-1} (ν_1PO_4), which corresponds to the relative amount of carbonate over the mineral amount; 5) crystallinity defined as the inverse of the full width at half maximum intensity of the ν_1PO_4 band, which reflects the size and perfection of crystals of hydroxyapatite.

2.10. Statistical analysis

Statistical analyses were performed using Prism 5 (GraphPad). Normal distribution of data was determined using either the Shapiro-Wilk normality test or the D'Agostino & Pearson omnibus test according to the sample size. Normally distributed data were analyzed using unpaired-*t*-test and two-way ANOVA; otherwise nonparametric Mann–Whitney tests were used as stated. $p < 0.05$ was considered significant. Data are presented as the means ± standard errors of the means (*i.e.*, SEM) from at least two independent experiments performed using two to four distinct donors as indicated.

3. Results

3.1. Obtention and validation of the devitalized ECMs from human BMAds at low and high glucose concentrations

To investigate the impact of ECM generated *in vitro* from mature human BMAds under hyperglycemic condition, human BM-MSCs were differentiated for up to 21 days in adipogenic media containing either 5.5 mM (LG) or 25 mM (HG) glucose, according to our previous study (Rharass and Lucas, 2019) (Fig. 1A). In agreement with our earlier work, glucose concentration did not induce any changes in the commitment to adipogenesis, and between the 14th and 21st days, BMAds equally accumulated triglycerides in the LG and HG conditions, regardless of the donor (Fig. 2A).

Among the different devitalization methods, the use of a hypotonic solution such as demineralized sterile water was found to be the most efficient and the gentlest to rupture cells without altering the produced matrix, as already reported (Mendibil et al., 2020; Wang et al., 2013) (Fig. 1B). Following treatment with DNase and lipase, no more staining of nuclear residues or lipid droplets on either ECM_{BMAd} LG or ECM_{BMAd} HG was observed (Fig. 2A), which confirmed the removal of cellular components. Measurements (Supplemental Fig. S1) and visualization of proteins contained in the two types of ECM_{BMAd} (following SDS–PAGE electrophoresis and silver nitrate staining) confirmed the presence of high- and low-molecular-weight proteins (data not shown). In addition, Raman spectroscopy analyses demonstrated that the two ECM_{BMAd} displayed a similar composition compared to the ECM underlying the nondecellularized BMAds (as shown in Fig. 2B), indicating the good integrity of ECM_{BMAd} following the devitalization process. Moreover, the first Raman spectroscopy analyses revealed several differences in the composition of ECM_{BMAd} according to the glucose concentration used to

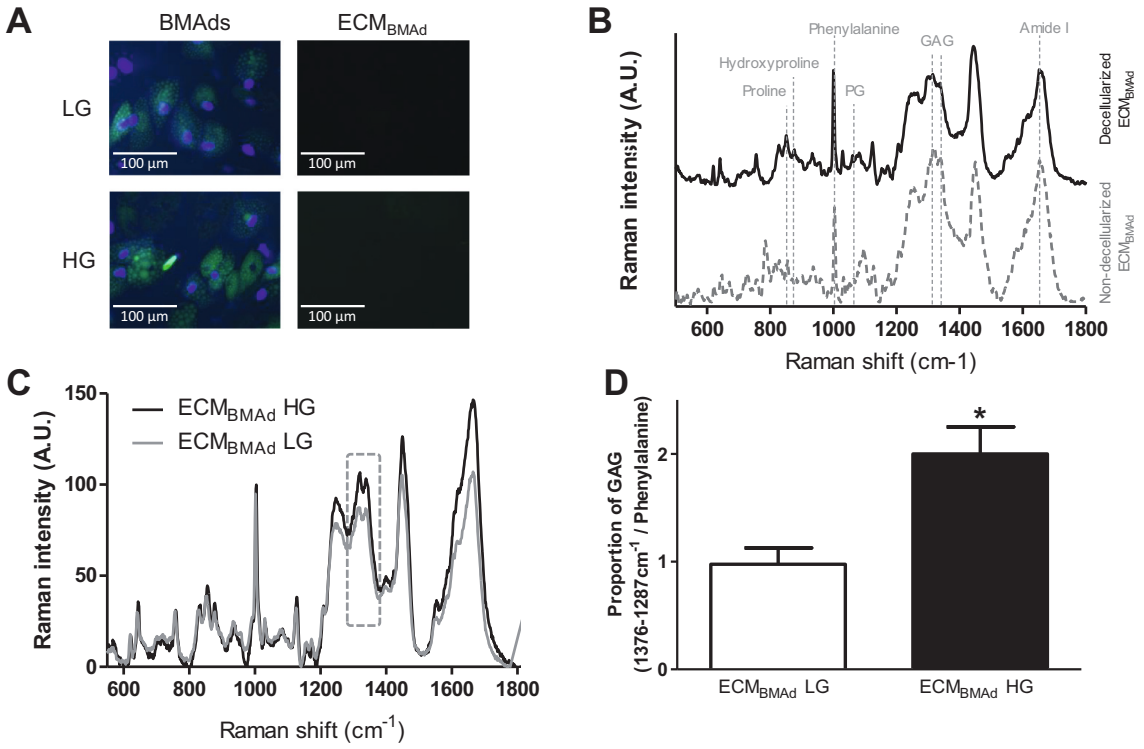

Fig. 2. Quality assessment of decellularized ECM_{BMAd}

Human BM-MSCs were differentiated into BMAds in either 5.5 mM (LG) or 25 mM (HG) glucose. After 21 days, cultures were decellularized to obtain the respective ECMs (ECM_{BMAd} LG and ECM_{BMAd} HG).

(A) Fluorescence microscopy images showing BMAds obtained in LG or HG concentrations and their respective ECM following the devitalization process. Nuclear labeling is shown in blue (DAPI), and triglyceride staining appears in green (BODIPY).

(B) Typical Raman spectra of the underlying layer of nondecellularized BMAds (dotted gray line, bottom) and decellularized ECM_{BMAd} (black line, top) are shown. Both were obtained under LG condition. The assignment of the major bands is indicated for peaks corresponding to the proline, hydroxyproline, phenylalanine and amide I groups for proteins (primarily collagens), proteoglycans (PG) and glycosaminoglycans (GAG). The same result was observed in HG condition.

(C) The mean Raman spectra of decellularized ECM_{BMAd} LG (light gray line) were overlaid with those of ECM_{BMAd} HG (black line) to highlight differences between the two types of ECM. As indicated by the frame, the proportion of GAGs is one of the major changes and (D) was determined as the ratio of the sum of the integrated areas of bands at 1318 and 1338 cm^{-1} to that of the phenylalanine band. The results are the means ± SEMs from 60 to 70 independent spectra from 2 donors. *$p <$ 0,05 using the Mann–Whitney test.

culture BMAds (Fig. 2C). The proportion of GAGs was quantified from individual Raman spectra and was significantly doubled in ECM_{BMAd} HG compared to ECM_{BMAd} LG (Fig. 2D). This result highlights a first change that could interfere with the proliferation and differentiation capacity of BM-MSCs (Chen et al., 2021). Of note, AGEs were detected but with no difference between the two types of ECM_{BMAd} (data not shown). Owing to the different profiles of adipocyte ECMs, both ECM_{BMAd} were used to analyze their impact on human BM-MSC behavior, commitment to osteoblastogenesis and quality of the resulting mineralized matrices.

3.2. *The matrices of BMAds favor BM-MSC attachment and proliferation*

Human BM-MSCs were seeded on ECM_{BMAd} LG, ECM_{BMAd} HG or plastic (control referred to as "without ECM") to study the impact of both adipocyte ECMs on adhesion and proliferation (Fig. 1C). The cell number was determined through DNA measurement. These parameters were only studied in the LG concentration since our study primarily aimed to analyze the effect of adipocyte matrices generated at two glucose concentrations on osteogenesis and, in that context, any preconditioning of human BM-MSCs by the HG condition during proliferation was avoided. Indeed, exposure of human BM-MSCs to HG can result in increased release of lactate dehydrogenase (an indicator of cytotoxicity) compared to exposure to the normoglycemic concentration, as observed in some donors (Supplementary Fig. S2A).

After 24 h of seeding, more cells (~15 %) adhered to both types of adipocyte matrices than to the control (Fig. 3A). Human BM-MSCs proliferated with culture time on all supports, yet an increase in the proliferation rate was observed between 2 and 4 days for the cells on ECM_{BMAd}, leading to a 24 % elevation in the cell number (Fig. 3B). mRNA expression levels of cyclin B1, one of the cell cycle regulatory proteins, were upregulated as early as 24 h in cells seeded on ECM_{BMAd}, whereas this increase only occurred after 48 h in cells without ECM (Fig. 3C). This finding corroborates better cell attachment and proliferation on BMAd matrices. Owing to the role of integrins in the interaction with surfaces and in the modulation of proliferation of human BM-MSCs (Lindner et al., 2010), expression levels of some of the primary subunits was analyzed. When comparing the influence of the different supports, *ITGA5* and *ITGB1* mRNA levels were found to be unmodified (Supplementary Fig. S2B and S2C). However, expression levels of *ITGAV* were surprisingly downregulated in cells on ECM_{BMAd} LG and partially in those on ECM_{BMAd} HG ($p = 0.09$) compared to cells without ECM at 48 h after seeding (Fig. 3D). This regulation could relate to an attempt by BM-MSCs to reduce their proliferation rate on ECM_{BMAd} but could also indicate an early commitment toward the adipocyte pathway (Morandi et al., 2016). However, mRNA levels of *PPARG*, the critical adipocyte transcription factor, were unchanged in cells on ECM_{BMAd} (Supplementary Fig. S2D), which discards a priming effect toward adipogenesis. As expected, the components of adipocyte ECMs favor cell attachment and proliferation. The ability of human BM-MSCs to differentiate into osteoblasts and to mineralize was then investigated ~48 h after seeding (60 % confluence) without ECM on ECM_{BMAd} LG or ECM_{BMAd} HG.

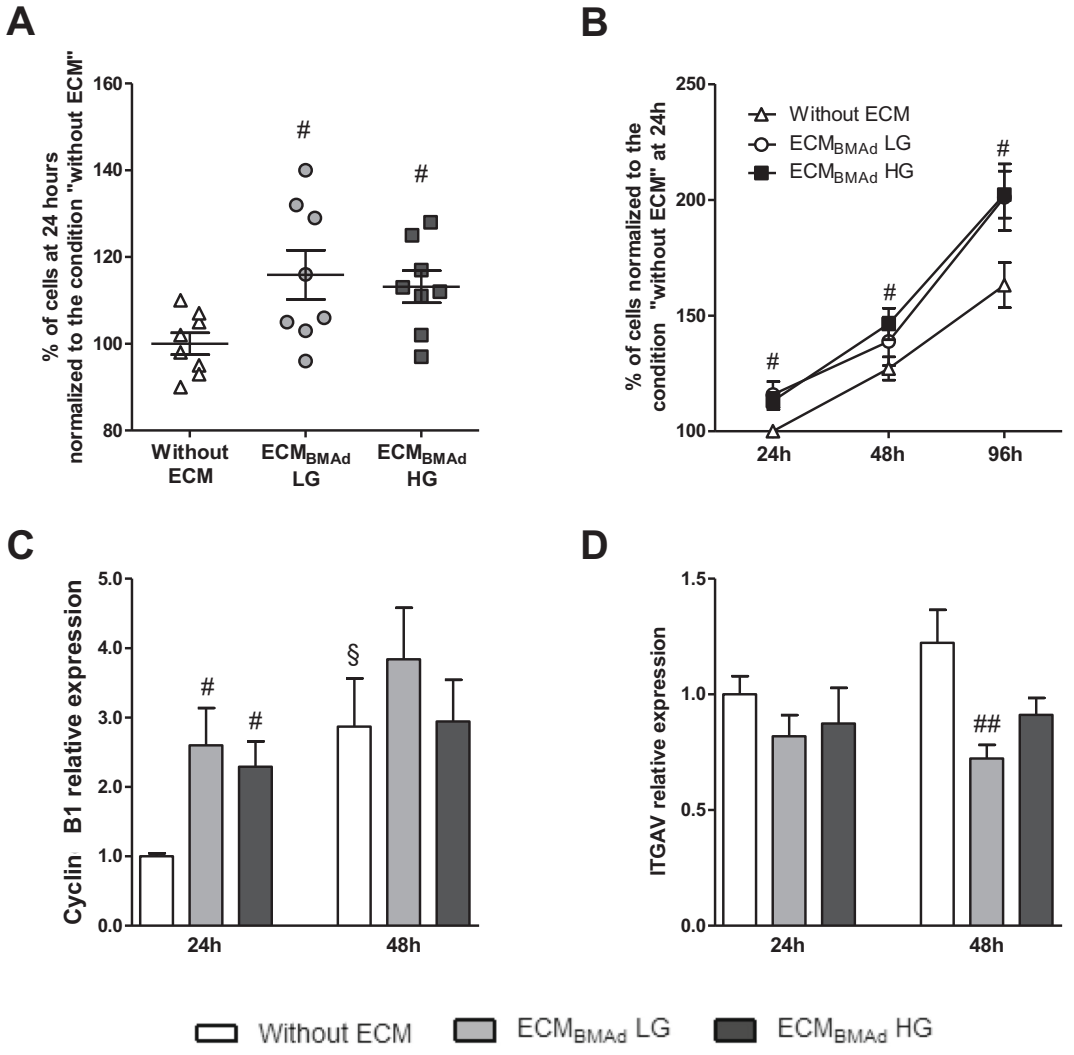

Fig. 3. Impact of adipocyte ECM on adhesion and proliferation of BM-MSCs.
BM-MSCs were seeded in complete LG medium, directly onto culture plates (without ECM, control) or on adipocyte ECMs generated either in 5.5 mM or 25 mM glucose (ECM_{BMAd} LG or ECM_{BMAd} HG, respectively). After 24, 48 and 96 h, DNA levels were measured and converted into cell number.
(A) Adhesion was assessed after 24 h, and (B) proliferation of cells was determined 48 and 96 h after seeding. The results are shown as the means ± SEMs from 8 independent experiments (4 donors) and are normalized to cell number at 24 h "without ECM". $^{\#}p < 0.05$, compared to "without ECM" for the same time, using unpaired *t*-test. Using 2-way ANOVA, significant differences were observed between 48 h and 96 h for ECM_{BMAd} LG *versus* without ECM ($p = 0{,}006$, Bonferroni posttests with $p < 0{,}05$ at 96 h) and for ECM_{BMAd} HG *versus* without ECM ($p = 0{,}025$, Bonferroni posttests with $p < 0{,}01$ at 96 h).
Gene expression was performed after 24 and 48 h for (C) cyclin B1 and (D) integrin alpha-V (*ITGAV*). The results are shown as the means ± SEMs from 8 independent experiments (4 donors) and are expressed according to *RPL13A* and normalized according to the condition "Without ECM at 24 hours" for each donor. $^{\#}p < 0.05$, $^{\#\#}p < 0.01$ compared to "without ECM" for the same timing; $^{\S}p < 0.05$ between 24 and 48 h for each condition of support, using Mann–Whitney tests.

3.3. High glucose concentration and adipocyte matrices do not alter osteoblastogenesis but reshape the expression pattern of mineralization-related genes

BM-MSC differentiation into osteoblasts was studied using the three support types and osteogenic medium containing either 5.5 mM glucose (LG), 25 mM glucose (HG) or 5.5 mM glucose and 20 mM mannitol (LGM, an osmolarity control) (Fig. 1.D). Expression levels of osteoblast markers was analyzed after 7 days, when commitment and differentiation toward the osteoblast lineage are primarily established, and after 16 days, when cell maturation and the mineralization process take place (Beck, 2003) (Fig. 4).

mRNA levels of RUNX2 were well expressed in all conditions and at both time points (Fig. 4A), while expression of the late marker osteocalcin (*OCN/BGLAP*) was similarly induced at 16 days regardless of the culture condition (Fig. 4B). *PPARG* mRNA levels were also unmodified by any of the culture conditions (Supplementary Fig. S3A). In addition, cell quantity was doubled on both ECM_{BMAd} compared to cells without ECM, confirming the maintenance of cell proliferation during osteoblastogenesis (Supplementary Fig. S3D). Altogether, these data support that BM-MSC differentiation into osteoblasts is not hampered by either hyperglycemic condition or adipocyte matrices.

The activity of osteoblasts was then assessed through mRNA expression analysis of several components of the mineralized matrix. First, expression levels of type 1 collagen (the primary isoform α1, *COL1A1*) was well induced by 7 days in all culture conditions, confirming unaltered differentiation (Fig. 4C). However, at this time, moderate alterations occurred for osteoblasts on ECM_{BMAd} LG and in LG concentration: mRNA levels were lower compared to osteoblasts without ECM or on ECM_{BMAd} HG. Moreover, *COL1A1* levels were upregulated by HG in osteoblasts on ECM_{BMAd} LG at the same time point. This glucose-induced alteration is observed for osteoblasts without ECM

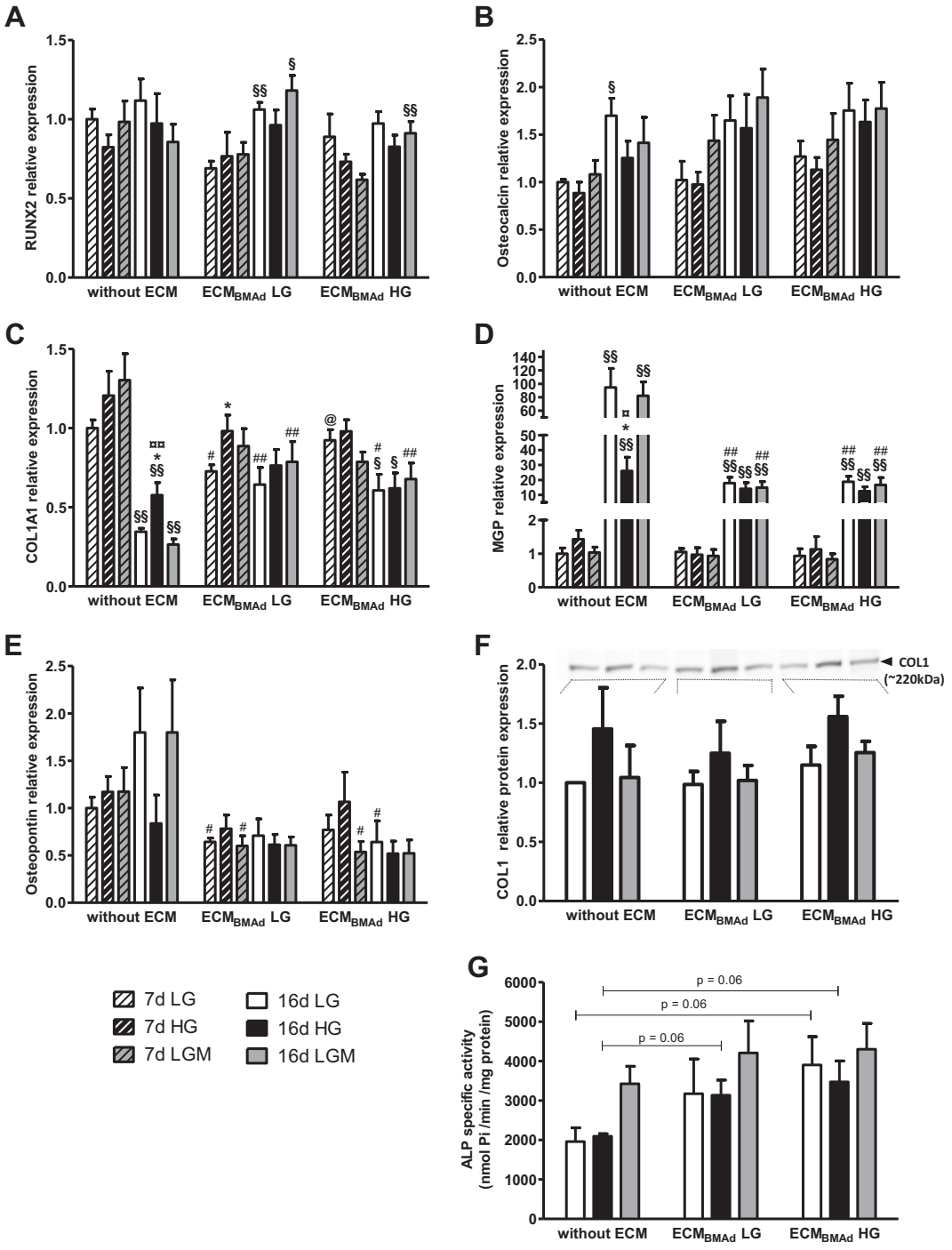

Fig. 4. Impact of glucose concentration and adipocyte ECM on osteoblastogenesis markers, mineralization-related genes and ALP activity.
BM-MSCs were seeded without ECM or on adipocyte ECM generated either in 5.5 mM or 25 mM glucose (ECM_{BMAd} LG or ECM_{BMAd} HG, respectively). After 48 h, the cells were differentiated in osteogenic medium containing either 5.5 mM (LG, white) or 25 mM (HG, black) glucose or 5.5 mM glucose +20 mM mannitol (LGM, gray).
Gene expression was measured after 7 days (hatched bars) and 16 days (filled bars) in osteogenic medium for (A) *RUNX2*, (B) Osteocalcin (*OCN*), (C) Collagen type I isoform a1 (*COL1A1*), (D) Matrix-Gla-Protein (*MGP*), and (E) Osteopontin (*OPN*).
The results are shown as the means ± SEMs from 6 independent experiments (3 donors) and are expressed according to *RPL13A* and normalized according to the condition "Without ECM in LG" for each donor. $^{\S}p < 0.05$, $^{\S\S}p < 0.01$ compared to 7 days for the same support and osteogenic medium; $^{*}p < 0.05$ compared to LG for the same support and timing; $^{¤}p < 0.05$, $^{¤¤}p < 0.01$ compared to LGM for the same support and timing; $^{\#}p < 0.05$, $^{\#\#}p < 0.01$ compared to "without ECM" for the same osteogenic medium and timing; $^{@}p < 0.05$, compared to ECM_{BMAd} LG for the same osteogenic medium and timing, using Mann–Whitney tests.
(F) Protein expression of collagen type I (COLI) was measured after 16 days in osteogenic medium. The results are shown as the means ± SEMs from 4 independent experiments (2 donors) and are expressed according to the sum of the intensities of Cy5-labeled proteins and normalized according to the condition "Without ECM in LG" for each experiment. A representative western blot of COLI detection (~220 kDa) is shown at the top.
(G) Alkaline phosphatase (ALP) activity was measured after 16 days and is expressed per level of proteins. The results are shown as the means ± SEMs from 4 independent experiments (2 donors). $p = 0.06$ for the indicated comparisons, using Mann–Whitney tests.

by 16 days: while *COL1A1* levels are substantially lowered as expected during this maturation phase (Beck, 2003), *COL1A1* levels are higher in the presence of 25 mM glucose compared to LG and LGM. *COL1A1* mRNA levels remained stable on ECM_{BMAd} LG or were slightly diminished on ECM_{BMAd} HG between the two time points. By 16 days, osteoblasts on both ECM_{BMAd} and cultured at HG concentration expressed similar RNA levels to those under LG and LGM conditions (Fig. 4C). To assess the impact of these different changes on the final protein amount of type I collagen, western blot analysis of osteoblasts and their deposited matrix was performed on the 16th day of culture (Fig. 4F). The total amount of COLI protein was unchanged regardless of the type of support. Of note, culture in HG resulted in a slight increase in COLI protein levels (2-way ANOVA assuming normal distribution and homogeneity of variance, $p = 0.03$ between LG and HG without any effect of the support).

Second, among other ECM components, attention has been given to the expression profile of matrix-Gla-protein (*MGP*), a glycoprotein considered to inhibit mineralization (Bonucci, 2012). *MGP* mRNA levels drastically rose during the maturation phase in all conditions (Fig. 4D). Culture without ECM and in HG reduced *MGP* expression levels by >3.5-fold compared to LG and LGM. Interestingly, *MGP* mRNA levels were similarly reduced when osteoblasts were cultured on any ECM_{BMAds} regardless of the glucose concentration. A comparable pattern was observed for osteopontin (*OPN/SPP1*), another glycoprotein with mineralization inhibiting properties (Bonucci, 2012) (Fig. 4E). Although one donor exhibited variability, *OPN* mRNA levels tended to increase by 16 days in osteogenic medium containing LG or LGM but remained low at HG concentration in the absence of adipocyte ECM. Compared to the situation without ECM, osteoblasts generated on ECM_{BMAd} globally exhibited diminished *OPN* expression levels at both time points without any clear impact of glucose concentration. In contrast, the expression analysis of osteonectin (*SPARC*) indicated a strong induction of this mineralization regulator (Bonucci, 2012) between 7 and 16 days, with no influence of glucose concentration or support type (Supplementary Fig. S3C).

Finally, to better characterize osteoblast phenotype, the specific activity of alkaline phosphatase (ALP) was measured after 16 days in osteogenic medium (Fig. 4G). The enzyme activity was unchanged by glucose concentration in the absence of ECM. Compared to these latter conditions, ALP activity tends to increase by 1.5- to 2-fold when osteoblasts were cultured on ECM_{BMAd}. Of note, ALP mRNA levels were not modified by culture conditions at 7 or 16 days (Supplementary Fig. S3B).

Collectively, these data strengthen that ECM_{BMAd} does not impair osteoblastogenesis but can alter the functional activity of osteoblasts.

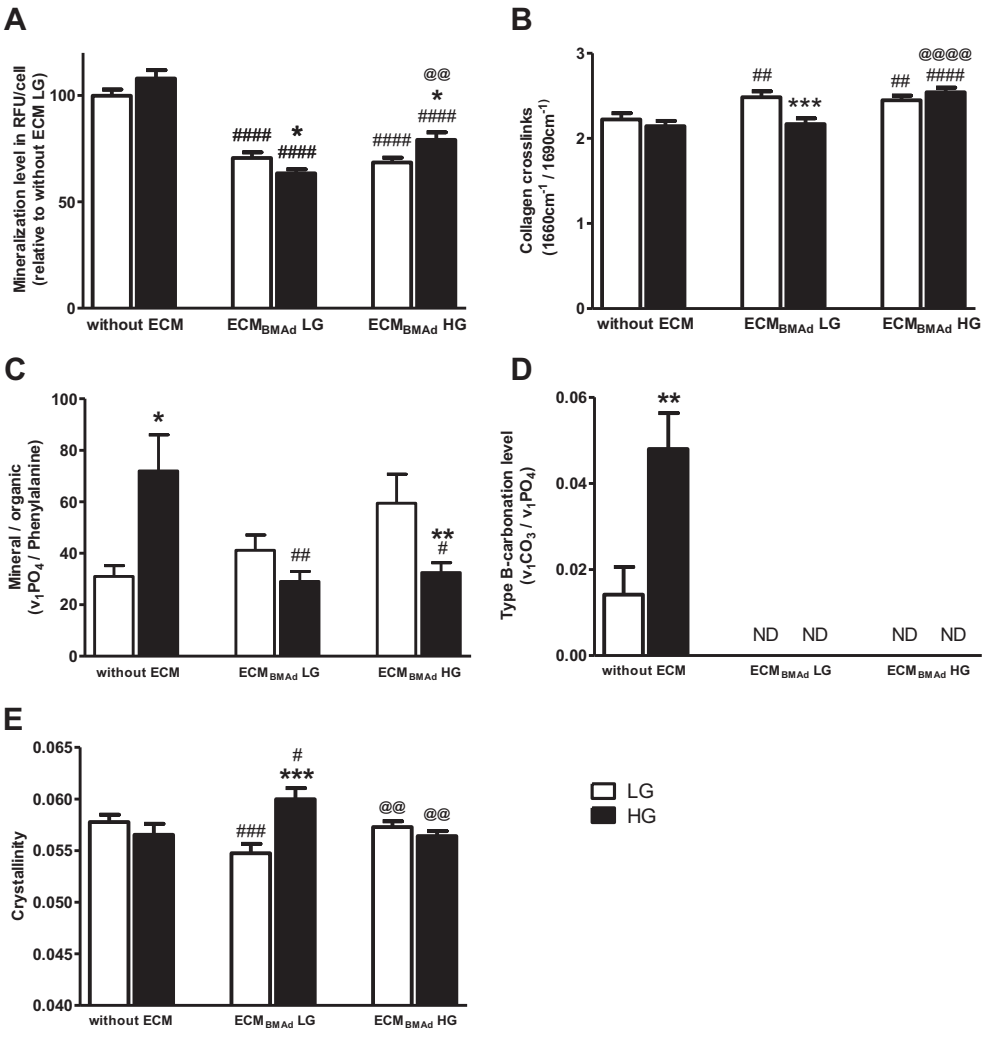

Fig. 5. Impact of glucose concentration and adipocyte ECM on mineralization parameters.

BM-MSCs were seeded without ECM or on adipocyte ECM generated either in 5.5 mM or 25 mM glucose (ECM_{BMAd} LG or ECM_{BMAd} HG, respectively) and differentiated in osteogenic medium containing either 5.5 mM (LG, white) or 25 mM (HG, black) glucose for 16 days.

(A) The mineralization achieved per cell was obtained after hydroxyapatite labeling and DNA measurement and is expressed according to the condition "Without ECM in LG" for each donor. The results are shown as the means ± SEMs from 32 independent experiments (4 donors). $^{\#\#\#\#}p < 0.0001$ compared to "without ECM" for the same osteogenic medium; $^{@@}p < 0.01$, compared to ECM_{BMAd} LG for the same osteogenic medium; $^{*}p < 0.05$ compared to LG for the same support, using Mann–Whitney tests.

(B) The collagen total crosslinks (determined as the ratio of the integrated area of the band at 1660 cm^{-1} to that of 1690 cm^{-1}), (C) the mineral to organic ratio (determined as the ratio of the integrated areas of v_1PO_4 to phenylalanine), (D) the level of type B-carbonate substitution (determined as the ratio of the integrated areas of v_1CO_3 to v_1PO_4) and (E) the crystallinity order of hydroxyapatite (determined from the full width at half height of the v_1PO_4 band) were measured using Raman spectroscopy. The results are shown as the means ± SEMs from at least 40 and up to 120 independent spectra, according to parameters (using 4 independent wells, 2 donors). $^{*}p < 0.05$, $^{**}p < 0.01$, $^{***}p < 0.001$ compared to LG for the same support; $^{\#}p < 0.05$, $^{\#\#\#}p < 0.001$, $^{\#\#\#\#}p < 0.0001$ compared to "without ECM" for the same osteogenic medium; $^{@@}p < 0.01$, $^{@@@@}p < 0.0001$ compared to ECM_{BMAd} LG for the same osteogenic medium, using Mann–Whitney tests. ND, not detected.

The gene expression analyses support that HG concentration also triggers alterations in the mineralization phase of osteoblasts without ECM. Some of these HG-induced changes are present when osteoblasts are grown on adipocyte matrices, as shown by COLI expression. In addition, the changes in *MGP* and *OPN* levels after 16 days of culture on both ECM_{BMAd} appear to be established in the LG concentration without further impact of the higher glucose concentration. Moreover, the specific effect of mannitol was rather comparable to the LG effect removing any strong impact of osmolarity, so the LGM condition was no longer included for subsequent analyses.

3.4. The quantity and quality of mineralization are altered in osteoblasts grown on adipocyte ECM

Osteoblast mineralization capacity was measured after 16 days using a fluorochrome that specifically binds to hydroxyapatite (HA) (Osteoimage) (Supplementary Fig. S4A). The cell count (obtained through DNA measurements) was considered given the increase in cell number on ECM_{BMAd} (Supplementary Fig. S3D). HA formation per cell was unchanged for osteoblasts generated without ECM when comparing the two glucose concentrations (Fig. 5A). Osteoblasts cultured on ECM_{BMAd} LG or ECM_{BMAd} HG exhibited severely decreased mineral formation compared to those cultured without ECM and regardless of glucose concentration. Of note, on these ECM_{BMAd}, the addition of 25 mM glucose slightly interfered with HA formation in an opposite manner; in the end, the HG condition triggered a mineralization level that was slightly higher on ECM_{BMAd} HG than that on ECM_{BMAd} LG. Overall, osteoblasts grown on ECM_{BMAd} LG or ECM_{BMAd} HG displayed a reduced ability to produce mineral, despite sustained or higher ALP activities, respectively (Fig. 4G).

Independent of the amount of mineralized tissue, the qualities of both the organic and the mineral matrix are important contributing factors in the determination of bone strength *in vivo*. The quality of mineralized nodules laid down by cells after 16 days was then characterized using Raman microspectroscopy as already used *in vitro* (McManus et al., 2011). The microscopic observation of nodules prior to analysis showed the presence of smaller nodules on both ECM_{BMAd} compared to those generated without ECM (data not shown), confirming the observed mineralization defects (Fig. 5A). Raman spectra of nodules showed the presence of bands assigned to mineral and organic matrix. The mineral bands were v_4PO_4 (580 cm^{-1}), v_1PO_4 (960 cm^{-1}) and v_1CO_3 (1070 cm^{-1}), which are characteristic of carbonated hydroxyapatite (Supplementary Fig. S4C). The organic matrix is identified by the presence of bands of phenylalanine (1001 cm^{-1}), amide III (1257 cm^{-1}) and amide I (1657 cm^{-1}), which are characteristic of collagen I. The contents of collagen crosslinks (Fig. 5B) and pyridinoline trivalent crosslinks (Supplementary Fig. S4B) were first determined from amide I band based on the method of Gamsjaeger and coll. (Gamsjaeger et al., 2017). Compared to conditions without ECM, the levels of collagen crosslinks were increased in the presence of ECM_{BMAd}. Cultures in HG did not modify collagen crosslinks in the absence of ECM but caused a different response depending on the adipocyte matrix. These post-translational modifications in collagen appeared the most pronounced on the ECM_{BMAd} HG: the levels of crosslinking were not increased by the high concentration of glucose in the osteogenic medium but were significantly amplified at this glucose concentration compared to the ECM_{BMAd} LG. On the ECM_{BMAd} LG, exposure to the LG concentration also triggered an elevation in both types of collagen crosslinking, while exposure to HG lowers them. Altogether, these data indicate that changes in glucose levels during osteoblast development are not the primary cause impacting collagen processing. Moreover, the matrix formed by BMAds exposed to the HG concentration could interfere more prominently with this process than those generated under the LG condition.

The mineral to organic ratio was next determined through the ratio of the integrated areas of v_1PO_4 to phenylalanine. This parameter exhibited striking differences according to culture conditions (Fig. 5C). Matrix mineralization significantly increased (by 2-fold) in HG compared to LG in the absence of ECM. At LG concentration, matrix mineralization also tended to increase on ECM_{BMAd} HG compared to the situations without ECM (by 92 %, $p = 0.08$) and ECM_{BMAd} LG (by 42 %, $p = 0.08$). However, at HG concentration, matrix mineralization was reduced in both ECM_{BMAd} compared to that without ECM. This reduction was also observed (by 45 %) when comparing the HG and LG concentrations on ECM_{BMAd} HG. Considering that the expression levels of COLI (the matrix component primarily mineralized) was relatively similar in HG conditions regardless of the support type (Fig. 4F), these HG-mediated perturbations most likely result from alterations in HA deposits within collagen fibrils.

The levels of type-B carbonate were also affected according to the culture conditions (Fig. 5D). In the condition without ECM, type-B carbonate substitution level was increased by 3.4-fold in HG compared to LG concentration. Remarkably, on both ECM_{BMAds} and regardless of glucose concentration, no carbonate substitution of hydroxyapatite was detected.

Finally, the crystallinity parameter was also assessed under all conditions (Fig. 5E). This parameter depends on the size of crystallites and/or the degree of order of the ions within the crystal lattice. Crystallinity is not modified by the glucose concentration in the absence of ECM. In addition, in the ECM_{BMAd} LG condition, crystallinity was the lowest in LG concentration and the highest in HG concentration compared to the two other supports.

Taken together, these data reveal that adipocyte matrices alter the phase of mineralization of osteoblasts. Osteoblast culture on any ECM_{BMAds} reduces the quantity of mineral laid down per cell, and the quality of both the organic matrix and the mineral is impaired. Moreover, some of these ECM_{BMAd}-induced changes differ from those induced by HG in the absence of ECM.

4. Discussion

BMAds are considered active cells that participate in the formation and resorption of bone by interfering with osteoblastogenesis and releasing various regulatory factors. In this study, we aimed to decipher the contribution of the ECM of mature BMAds in the context of chronic hyperglycemia. Using osmotic shock followed by DNase and lipase treatment, BMAds-free ECMs exhibited a similar general composition as the native matrix with adipocytes, indicating preservation of the matrix composition after devitalization. Regardless of the glucose concentration provided during the differentiation and maturation of adipocytes, the matrices of BMAds favored the attachment and proliferation of BM-MSCs and did not prevent their commitment toward the osteoblast lineage. However, adipocyte matrices altered the maturation and mineralization phase of osteoblasts, resulting in a low quantity and disturbed quality of mineralization. In contrast to exposure to HG, the adipocyte matrices provide an environment that specifically prevents carbonate substitution of the mineral and favors collagen crosslinking. Moreover, the mineral to organic ratio was disturbed according to the presence of adipocyte ECMs and the glucose concentration used during the culture of adipocytes or osteoblasts. Our results highlight that HG concentration and ECM_{BMAd} can lead to different defects within the mineralization quality and should both be considered in the compromised bone quality of T2D.

Higher adhesion and proliferation of human BM-MSCs on various ECMs compared to plastic surface are quite common (Baroncelli et al., 2018b; Lindner et al., 2010). Compared to these studies, our two types of ECM_{BMAd} moderately promoted the proliferation rate of human BM-MSCs. However, our results differ from previous work showing no impact of the ECM generated from human BM-MSC-derived BMAds on these parameters (Hoshiba et al., 2010). This discrepancy may result from the use of more mature BMAds (following 21 days in adipogenic medium), which can affect the deposition of matrix components that

were also obtained through a different and gentler process. We acknowledge that direct comparison to ECM from other cells, such as BM-MSCs, could have been beneficial in better characterizing the effects of ECM_{BMAd}. However, compared to these earlier studies (Baroncelli et al., 2018b; Hoshiba et al., 2010), we used multiple donors (2 females and 2 males), which, owing to variability between individuals, is likely to reflect more generalizable responses. Finally, apart from promoting BM-MSC attachment and proliferation, no early commitment toward adipogenesis or osteoblastogenesis was observed.

Gene expression analyses of the early and late osteogenic markers *RUNX2* and *OCN*, the adipogenic marker *PPARG*, and measurements of COLI and ALP activity demonstrated that adipocyte matrices, regardless of the glucose concentration used during the adipogenic process, did not affect the commitment and differentiation of BM-MSCs toward the osteoblast lineage, even in the presence of 25 mM glucose. First, these results seem surprising in light of several factors secreted by BMAds that can inhibit osteoblastogenesis (Rharass and Lucas, 2018) and could be retained by the ECM. Second, the ECM composition itself is expected to modify BM-MSC commitment and differentiation (Hoshiba et al., 2016), and the change in GAG content between the two ECM_{BMAds} could have modulated the cell response (Chen et al., 2021). However, another independent study reported that the ECM generated after either early or later stages of adipogenesis (3 and 10 days, respectively) does not perturb osteoblastogenesis: human BM-MSC-derived osteoblasts differentiated either on these adipocyte ECMs or osteoblast ECM display similar ALP staining and *RUNX2* and *OPN* mRNA expression (Hoshiba et al., 2012). In addition, this same group also demonstrated that only the ECM produced by early adipocytes, and not that generated by late adipocytes, promotes adipogenesis (Hoshiba et al., 2010, 2012). Using matrices generated from even more mature adipocytes and according to another devitalization method, our study thus strengthens the notion that the matrix of BMAds does not predominantly interfere with osteoblastic differentiation. Nevertheless, one must keep in mind that these results are derived from *in vitro* studies for which the differentiation medium has been developed to maximize the stimulation of osteogenic differentiation, which could mitigate the effect of important components in a more pathophysiological context.

Third, HG has been demonstrated to drastically inhibit osteoblast differentiation in the human osteoblast MG-63 cell line (Shao et al., 2014; Wang et al., 2010) and in primary rat osteoblasts (Zhang and Yang, 2013), leading to a shift toward adipogenesis. However, divergent results have been obtained for human BM-MSCs with either decreased (Keats and Khan, 2012) or unchanged (Hankamolsiri et al., 2016) osteoblastogenesis in the presence of 25 mM glucose compared to the normoglycemic condition. In this context, our data support that HG may not interfere with human BM-MSC commitment and differentiation toward the osteogenic lineage and that their culture on ECM_{BMAd} does not sensitize them to the potential anti-osteoblastic effects of HG. Importantly, it is during their maturation and mineralizing stage that osteoblasts become responsive to HG concentration and to adipocyte matrices.

Changes in the expression levels of *COL1A1*, *MGP* and *OPN* were observed on the 16th day in osteoblasts obtained on ECM_{BMAd} and for those cultured on plastic in HG condition. Despite a sustained or even higher ALP activity and the downregulation of two mineralization inhibitors, these changes resulted in much lower mineralizing ability of osteoblasts on adipocyte matrices regardless of glucose concentration. However, as previously reported (Baroncelli et al., 2018a; Botolin and McCabe, 2006; Blair et al., 2017; Schäck et al., 2013), ALP activity levels are not always proportional to the degree of mineralization of cells. In addition, as discussed in the last paragraph, *MGP* and *OPN* transcription could be regulated by other environmental cues. Regarding the impact of HG concentration, *in vitro* data are quite divergent, showing either reduced (Balint et al., 2001; Cunha et al., 2014), higher (García-Hernández et al., 2012) or unchanged (Botolin and McCabe, 2006) mineralization levels. However, two of these studies revealed that increased glucose concentration interferes with the mineralization process (Balint et al., 2001; García-Hernández et al., 2012). The quality of the mineral has begun to be analyzed, and a diminished calcium to phosphorus ratio induced at HG concentration was reported (García-Hernández et al., 2012). This led us to further characterize the mineralization quality using Raman spectrometry, which revealed alterations more specific to the type of support or to the glucose concentration used.

In the absence of ECM and compared to normoglycemic condition, the mineralized matrix generated in the HG concentration displayed an increase in the mineral-to-matrix ratio and the type-B carbonate substitution level. The latter alteration (corresponding to a substitution of a phosphate by a carbonate group) is in agreement with the reduced calcium to phosphorus ratio already mentioned (García-Hernández et al., 2012) and has also been recently reported using a human osteoblast cell line (Cifuentes-Mendiola et al., 2022). Increased mineralization of the organic matrix is a feature of the cortical region of long bones in most rodent models of T2D (Creecy et al., 2016; Hammond et al., 2014; Hunt et al., 2018). The HG condition without ECM thus mimics some of the defects in bone quality observed in T2D. Interestingly, on ECM_{BMAd} HG and following exposure to LG, such an elevation in the mineral to organic ratio also occurred. This suggests that the ECM provided by BMAds previously exposed to an HG concentration perturbs the mineral deposition even if the subsequent concentration of glucose is not deleterious. Surprisingly, however, when osteoblasts were exposed to both ECM_{BMAd} and HG concentration, the mineral to organic ratios appeared to be restored to the levels observed in control (without ECM in LG condition) and were significantly decreased compared to the conditions without ECM in HG and ECM_{BMAd} HG in LG. In fact, a decrease in this ratio has also been reported at sites of bone formation in a T2D model (Mieczkowska et al., 2020), suggesting that such defects can appear early in diabetes. In addition, one can consider that BMAds primarily develop in close vicinity to the trabeculae and that changes often reported for the cortical at midshaft of long bones may be not representative. In that context, it should be emphasized that the mineral to organic ratio for the trabecular compartment is quite low compared to the cortical compartment and is unchanged by diabetes or obese status (Hunt et al., 2018; Marin et al., 2018).

Moreover, two other modifications are specifically triggered in the presence of adipocyte matrices. First, both total and trivalent crosslink levels of collagen are increased when osteoblasts are differentiated on ECM_{BMAd}. These enzyme-mediated crosslinkings of collagen are related to the way matrix collagen molecules are arranged and stabilized in fibrils, which results in different mechanical properties of the organic matrix and plays a role in bone toughness and strength (Viguet-Carrin et al., 2006). Of note, the nonenzymatic formation of AGEs, which is also considered to impair bone quality (Lekkala et al., 2019; Viguet-Carrin et al., 2006), could not be reliably measured in our experiments. Enzymatic crosslink formation has been reported to be both decreased (Mieczkowska et al., 2020; Saito et al., 2006) and increased (Creecy et al., 2018; Hunt et al., 2018) in the bones of different T2D models. However, our set of experiments supports that the differentiation and maturation of osteoblasts on any ECM_{BMAds} have a greater impact on this parameter than the HG concentration exposure itself. In this regard, it must be mentioned that collagen maturity is positively correlated with age (Boskey and Imbert, 2017) and is increased in various postmenopausal animal models (Pezzotti et al., 2017; Wen et al., 2015) as well as in human bones of different osteoporotic types (Bätge et al., 1992; Garcia et al., 2016; Paschalis et al., 2004) compared to controls. A raise in collagen maturity has been associated with impaired bone mechanical properties (Pezzotti et al., 2017; Wen et al., 2015) and fragility fractures (Gourion-Arsiquaud et al., 2009; Rokidi et al., 2019). Altogether, our results strongly suggest that BMAds indirectly contribute, through their ECM, to alterations of the new bone collagen matrix produced in osteoporosis. This deleterious contribution could also occur in T2D: although the effects of the HG concentration on ECM_{BMAd} LG are difficult to interpret, our results indeed infer that the ECM produced by

BMAds chronically exposed to hyperglycemia can perturb the osteoblast processing of the organic matrix independently of the glucose concentration thereafter.

The second striking feature of the mineral generated on both ECM_{BMAd} is the absence of type-B carbonate, which is characteristic of biological apatite in bone. Raman spectroscopy has been shown to be very sensitive for determining the amount of type-B carbonate (Penel et al., 1998). This carbonate substitution occurs *in vitro* with human BM-MSC-derived osteoblasts, as shown in our control experiments (without ECM) and by Schäck and colleagues (Schäck et al., 2013) with an increasing rate of formation between 14 and 21 days of culture (McManus et al., 2011). Of note, in a culture medium allowing both adipogenesis and osteogenesis of murine bone marrow stromal cells, the formed HA was also devoid of any carbonate (Ghali et al., 2015) (G. Falgayrac, personal communication). Altogether, these data support that the presence of BMAd factors in the microenvironment of differentiating and maturing osteoblasts prevents the carbonate substitution of apatite.

As previously observed for other criteria, carbonate substitution level is highly variable and appears to increase (Tice et al., 2021), remain unchanged (Creecy et al., 2016; Hammond et al., 2014; Hunt et al., 2018) or decrease (Creecy et al., 2018; Mieczkowska et al., 2020) in T2D models. In contrast, we (Fig. 5D) and others (Cifuentes-Mendiola et al., 2022) show that HG exposure alone results in a higher carbonate substitution level; which indicates that other mechanisms are involved to modulate such change within the mineral. It should be noted that continuous insulin administration decreases the type B carbonate substitution in the bones of T2D rats independently of the restoration of glycemia, suggesting that lack of insulin effect may also be implicated in such defects (Shi et al., 2021). The consequences of carbonate substitution on bone mechanical properties (Unal et al., 2018) and fracture resistance (Gourion-Arsiquaud et al., 2009; Boskey et al., 2016; Mandair et al., 2021) are still controversial and continue to be investigated. This type of substitution has been reported to be negatively associated with crystallinity (Deymier et al., 2017; Yerramshetty et al., 2006), another parameter potentially interfering with bone quality (Unal et al., 2018). However, as also described in other studies (Boskey and Imbert, 2017; Boskey et al., 2016), the expected changes in crystallinity were not observed in relation to the lack of carbonate substitution in our experiments. The use of synthetic hydroxyapatites also provides interesting insights regarding the biological effect of different carbonate contents, which can affect the proliferation and differentiation of osteoblast-like cells (Adams et al., 2014; Germaini et al., 2017; Rupani et al., 2012) as well as the rate of resorption (Germaini et al., 2017). Although the outcomes of changes in carbonate substitution in the bone mechanical properties have yet to be clarified, our study underlines the importance of the ECM produced by BMAds, which can prevent this substitution in the apatite crystal. In addition to quantity, bone composition plays a crucial role in the mechanical properties and fragility of bone. However, their interrelationships are difficult to assess since these different bone constituents differ with age, disease state, bone site (*i.e.*, metaphysis or diaphysis) and bone compartment (cortical or trabecular) (Boskey and Imbert, 2017). In that respect, the use of *in vitro* models, and more particularly devitalized matrices (Hoshiba et al., 2016), provides key clues regarding the relative importance of cells and their microenvironment in bone changes. Our study demonstrated that BMAds interfere with bone quantity and quality through the production of their ECM. For osteoblasts grown on these adipocyte matrices, the mineralization process alterations diverge from those triggered by the HG condition only. The extension level of the mineral to the matrix, the collagen maturity and the degree of carbonate substitution were modified in the presence of the BMAd microenvironment. Considering the relevance of these parameters in T2D and in osteoporosis more generally, our study should stimulate the appraisal of the presence of BMAds to better decipher the underlying mechanisms in bone quality. Defects in mineral deposition by osteoblasts grown on ECM_{BMAd} are, at the cellular (Fig. 5A) and molecular (Fig. 5C) levels, partly dependent on the glucose concentration to which BMAds and then osteoblasts are exposed. The quantity of produced COL1 is unlikely to be implicated: regardless of the type of support, the amount of COLI protein is similar in LG condition and increases during HG exposure, as previously reported (Botolin and McCabe, 2006; Cunha et al., 2014). However, other mechanisms, such as acidosis, can be involved. Acidosis strongly inhibits mineralization of the matrix produced by osteoblasts (Brandao-Burch et al., 2005). Indeed, a low pH inhibits ALP activity (Brandao-Burch et al., 2005), decreases bone carbonate content (Bushinsky et al., 1993) and down-regulates mRNA levels of both *MGP* (Frick and Bushinsky, 1999) and *OPN* (Brandao-Burch et al., 2005; Frick and Bushinsky, 1999). Deposition of hydroxyapatite onto collagen is also highly dependent on the control of the pH, which should remain at ~pH 7.4 (Schlesinger et al., 2019). Importantly, exposure of osteoblasts to an HG concentration results in acidification of the medium (Botolin and McCabe, 2006). In our study, osteoblasts grown on ECM_{BMAd} (regardless of glucose concentration) display a comparable decrease in the expression of *MGP* and *OPN* to osteoblasts cultured in HG and lay down a mineral with no carbonate. Considering the environmental acidification associated with adipocyte metabolism (Civelek et al., 1996; Sabater et al., 2014), one can speculate that BMAds provide an acidic microenvironment leading to the observed alterations. Subsequent exposure of osteoblasts on ECM_{BMAd} to the HG concentration could further lower pH and result in a severe decrease in mineral deposit, as observed (Fig. 5C). This interesting hypothesis linking several outcomes of our study deserves further investigation.

5. Conclusions

Our study shows for the first time that the ECM produced by human BMAds affects both bone quantity and quality. The ECMs of BMAds, independent of the glucose concentration to which they were exposed, do not impair the commitment of BM-MSCs in osteoblastogenesis but do disrupt the mineralization phase of osteoblasts. In addition to decreased cell mineralization, culture of osteoblasts on adipocyte ECMs results in abnormal mineralized nodules with increased collagen crosslinks and no type-B carbonate substitution. Moreover, glucose concentration primarily interferes with the mineral to organic ratio with divergent outcomes according to culture conditions. Our results highlight that HG concentration and adipocyte ECM result in differential alterations in mineralization quality, which, yet, recapitulates the contradictory changes observed in T2D osteoporosis. Given the rising need for a better understanding of bone composition, our study sheds light on the importance of BMAd involvement, which should be considered in the compromised bone quality of T2D and osteoporosis patients more generally.

Funding

LE was supported by the University of Littoral Côte d'Opale (ULCO) through a doctoral fellowship.

This work was supported by the MSD AVENIR Foundation [ADIMETABONE project] to SL.

CRediT authorship contribution statement

Laura Entz: Investigation; Methodology; Formal analysis; Validation; Writing - review & editing.

Guillaume Falgayrac: Data curation; Formal analysis; Validation; Methodology (Raman); Writing - review & editing.

Christophe Chauveau: Resources; Writing - review & editing.

Gilles Pasquier: Supervision; Writing - review & editing.

Stéphanie Lucas: Conceptualization; Supervision; Validation; Funding acquisition; Project administration; Resources; Writing - original draft.

Declaration of competing interest

The authors declare the following financial interests/personal relationships which may be considered as potential competing interests:

Stephanie LUCAS reports financial support was provided by MSD Avenir Foundation.

Data availability

Data will be made available on request.

Acknowledgments

The authors are grateful to Dr. Tareck Rharass for his valuable comments regarding the manuscript and Dr. Guillaume Duflos (ANSES, Boulogne sur Mer, France) for providing the spectrofluorometer facility. We acknowledge the University of Littoral Côte d'Opale (ULCO) for its support during the COVID-19 pandemic.

Appendix A. Supplementary data

Supplementary data to this article can be found online at https://doi.org/10.1016/j.bonr.2022.101622.

References

Adams, B.R., Mostafa, A., Schwartz, Z., Boyan, B.D., 2014. Osteoblast response to nanocrystalline calcium hydroxyapatite depends on carbonate content. J. Biomed. Mater. Res. A 102, 3237–3242. https://doi.org/10.1002/jbm.a.34994.

Andrade, V.F.C., Besen, D., Chula, D.C., Borba, V.Z.C., Dempster, D., Ca, M., 2021. Bone marrow adiposity in premenopausal women with type 2 diabetes with observations on peri-trabecular adipocytes [WWW document]. J. Clin. Endocrinol. Metab. https://doi.org/10.1210/clinem/dgab322.

Balint, E., Szabo, P., Marshall, C.F., Sprague, S.M., 2001. Glucose-induced inhibition of in vitro bone mineralization. Bone 28, 21–28.

Baroncelli, M., van der Eerden, B.C., Kan, Y.-Y., Alves, R.D., Demmers, J.A., van de Peppel, J., van Leeuwen, J.P., 2018. Comparative proteomic profiling of human osteoblast-derived extracellular matrices identifies proteins involved in mesenchymal stromal cell osteogenic differentiation and mineralization. J. Cell. Physiol. 233, 387–395. https://doi.org/10.1002/jcp.25898.

Baroncelli, M., van der Eerden, B.C.J., Chatterji, S., Rull Trinidad, E., Kan, Y.Y., Koedam, M., van Hengel, I.A.J., Rdam, Alves, Fratila-Apachitei, L.E., Demmers, J.A. A., van de Peppel, J., van Leeuwen, J.P.T.M., 2018. Human osteoblast-derived extracellular matrix with high homology to bone proteome is osteopromotive [WWW document]. Tissue Eng. A. https://doi.org/10.1089/ten.TEA.2017.0448.

Bätge, B., Diebold, J., Stein, H., Bodo, M., Müller, P.K., 1992. Compositional analysis of the collagenous bone matrix. A study on adult normal and osteopenic bone tissue [WWW document]. Eur. J. Clin. Invest. https://doi.org/10.1111/j.1365-2362.1992.tb01450.x.

Beck, G.R., 2003. Inorganic phosphate as a signaling molecule in osteoblast differentiation. J. Cell. Biochem. 90, 234–243. https://doi.org/10.1002/jcb.10622.

Blair, H.C., Larrouture, Q.C., Li, Y., Lin, H., Beer-Stoltz, D., Liu, L., Tuan, R.S., Robinson, L.J., Schlesinger, P.H., Nelson, D.J., 2017. Osteoblast differentiation and bone matrix formation in vivo and in vitro. Tissue Eng. B Rev. 23, 268–280. https://doi.org/10.1089/ten.teb.2016.0454.

Bonucci, E., 2012. Bone mineralization. Front. Biosci. Landmark Ed. 17, 100–128. https://doi.org/10.2741/3918.

Boskey, A.L., Imbert, L., 2017. Bone quality changes associated with aging and disease: a review. Ann. N. Y. Acad. Sci. 1410, 93–106. https://doi.org/10.1111/nyas.13572.

Boskey, A.L., Donnelly, E., Boskey, E., Spevak, L., Ma, Y., Zhang, W., Lappe, J., Recker, R. R., 2016. Examining the relationships between bone tissue composition, compositional heterogeneity, and fragility fracture: a matched case-controlled FTIRI study. J. Bone Miner. Res. Off. J. Am. Soc. Bone Miner. Res. 31, 1070–1081. https://doi.org/10.1002/jbmr.2759.

Botolin, S., McCabe, L.R., 2006. Chronic hyperglycemia modulates osteoblast gene expression through osmotic and non-osmotic pathways. J. Cell. Biochem. 99, 411–424. https://doi.org/10.1002/jcb.20842.

Brandao-Burch, A., Utting, J.C., Orriss, I.R., Arnett, T.R., 2005. Acidosis inhibits bone formation by osteoblasts in vitro by preventing mineralization. Calcif. Tissue Int. 77, 167–174. https://doi.org/10.1007/s00223-004-0285-8.

Bushinsky, D.A., Lam, B.C., Nespeca, R., Sessler, N.E., Grynpas, M.D., 1993. Decreased bone carbonate content in response to metabolic, but not respiratory, acidosis. Am. J. Phys. 265, F530–F536. https://doi.org/10.1152/ajprenal.1993.265.4.F530.

Chaves Neto, A.H., Brito, V.G.B., Landim de Barros, T., do Amaral, C.C.F., Sumida, D.H., Oliveira, S.H.P., 2018. Chronic high glucose and insulin stimulate bone-marrow stromal cells adipogenic differentiation in young spontaneously hypertensive rats. J. Cell. Physiol. 233, 6853–6865. https://doi.org/10.1002/jcp.26445.

Chen, X.-D., Dusevich, V., Feng, J.Q., Manolagas, S.C., Jilka, R.L., 2007. Extracellular matrix made by bone marrow cells facilitates expansion of marrow-derived mesenchymal progenitor cells and prevents their differentiation into osteoblasts. J. Bone Miner. Res. Off. J. Am. Soc. Bone Miner. Res. 22, 1943–1956. https://doi.org/10.1359/jbmr.070725.

Chen, J., Sun, T., You, Y., Wu, B., Wang, X., Wu, J., 2021. Proteoglycans and glycosaminoglycans in stem cell homeostasis and bone tissue regeneration. Front. Cell Dev. Biol. 9, 760532 https://doi.org/10.3389/fcell.2021.760532.

Chuang, C.C., Yang, R.S., Tsai, K.S., Ho, F.M., Liu, S.H., 2007. Hyperglycemia enhances adipogenic induction of lipid accumulation: involvement of extracellular signal-regulated protein kinase 1/2, phosphoinositide 3-kinase/Akt, and peroxisome proliferator-activated receptor gamma signaling. Endocrinology 148, 4267–4275. https://doi.org/10.1210/en.2007-0179.

Cifuentes-Mendiola, S.E., Moreno-Fierros, L., González-Alva, P., García-Hernández, A.L., 2022. Docosahexaenoic acid improves altered mineralization proteins, the decreased quality of hydroxyapatite crystals and suppresses oxidative stress induced by high glucose [WWW Document]. Exp. Ther. Med. https://doi.org/10.3892/etm.2022.11160.

Civelek, V.N., Hamilton, J.A., Tornheim, K., Kelly, K.L., Corkey, B.E., 1996. Intracellular pH in adipocytes: effects of free fatty acid diffusion across the plasma membrane, lipolytic agonists, and insulin. Proc. Natl. Acad. Sci. U. S. A. 93 https://doi.org/10.1073/pnas.93.19.10139.

Craft, C.S., Scheller, E.L., 2016. Evolution of the marrow adipose tissue microenvironment. Calcif. Tissue Int. https://doi.org/10.1007/s00223-016-0168-9.

Creecy, A., Uppuganti, S., Merkel, A.R., O'Neal, D., Makowski, A.J., Granke, M., Voziyan, P., Nyman, J.S., 2016. Changes in the fracture resistance of bone with the progression of type 2 diabetes in the ZDSD rat. Calcif. Tissue Int. 99, 289–301. https://doi.org/10.1007/s00223-016-0149-z.

Creecy, A., Uppuganti, S., Unal, M., Clay Bunn, R., Voziyan, P., Nyman, J.S., 2018. Low bone toughness in the TallyHO model of juvenile type 2 diabetes does not worsen with age. Bone 110, 204–214. https://doi.org/10.1016/j.bone.2018.02.005.

Cunha, J.S., Ferreira, V.M., Maquigussa, E., Naves, M.A., Boim, M.A., 2014. Effects of high glucose and high insulin concentrations on osteoblast function in vitro. Cell Tissue Res. 358, 249–256. https://doi.org/10.1007/s00441-014-1913-x.

Deymier, A.C., Nair, A.K., Depalle, B., Qin, Z., Arcot, K., Drouet, C., Yoder, C.H., Buehler, M.J., Thomopoulos, S., Genin, G.M., Pasteris, J.D., 2017. Protein-free formation of bone-like apatite: new insights into the key role of carbonation. Biomaterials 127, 75–88. https://doi.org/10.1016/j.biomaterials.2017.02.029.

Ferland-McCollough, D., Masseli, D., Spinetti, G., Sambataro, M., Sullivan, N., Blom, A., Madeddu, P., 2018. MCP-1 feedback loop between adipocytes and mesenchymal stromal cells causes fat accumulation and contributes to hematopoietic stem cell rarefaction in the bone marrow of diabetic patients. Diabetes. https://doi.org/10.2337/db18-0044.

Frick, K.K., Bushinsky, D.A., 1999. In vitro metabolic and respiratory acidosis selectively inhibit osteoblastic matrix gene expression. Am. J. Phys. 277, F750–F755. https://doi.org/10.1152/ajprenal.1999.277.5.F750.

Gamsjaeger, S., Mendelsohn, R., Boskey, A.L., Gourion-Arsiquaud, S., Klaushofer, K., Paschalis, E.P., 2014. Vibrational spectroscopic imaging for the evaluation of matrix and mineral chemistry. Curr. Osteoporos. Rep. 12, 454–464. https://doi.org/10.1007/s11914-014-0238-8.

Gamsjaeger, S., Robins, S.P., Tatakis, D.N., Klaushofer, K., Paschalis, E.P., 2017. Identification of pyridinoline trivalent collagen cross-links by raman microspectroscopy [WWW document]. Calcif. Tissue Int. https://doi.org/10.1007/s00223-016-0232-5.

Garcia, I., Chiodo, V., Ma, Y., Boskey, A., 2016. Evidence of altered matrix composition in iliac crest biopsies from patients with idiopathic juvenile osteoporosis [WWW document]. Connect. Tissue Res. https://doi.org/10.3109/03008207.2015.1088531.

García-Hernández, A., Arzate, H., Gil-Chavarría, I., Rojo, R., Moreno-Fierros, L., 2012. High glucose concentrations alter the biomineralization process in human osteoblastic cells. Bone 50, 276–288. https://doi.org/10.1016/j.bone.2011.10.032.

Germaini, M.-M., Detsch, R., Grünewald, A., Magnaudeix, A., Lalloue, F., Boccaccini, A. R., Champion, E., 2017. Osteoblast and osteoclast responses to A/B type carbonate-substituted hydroxyapatite ceramics for bone regeneration. Biomed. Mater. Bristol Engl. 12, 035008 https://doi.org/10.1088/1748-605X/aa69c3.

Ghali, O., Broux, O., Falgayrac, G., Haren, N., van Leeuwen, J.P.T.M., Penel, G., Hardouin, P., Chauveau, C., 2015. Dexamethasone in osteogenic medium strongly induces adipocyte differentiation of mouse bone marrow stromal cells and increases osteoblast differentiation. BMC Cell Biol. 16, 9. https://doi.org/10.1186/s12860-015-0056-6.

Gourion-Arsiquaud, S., Faibish, D., Myers, E., Spevak, L., Compston, J., Hodsman, A., Shane, E., Recker, R.R., Boskey, E.R., Boskey, A.L., 2009. Use of FTIR spectroscopic imaging to identify parameters associated with fragility fracture [WWW document]. J. Bone Miner. Res. Off. J. Am. Soc. Bone Miner. Res. https://doi.org/10.1359/jbmr.090414.

Guneta, V., Zhou, Z., Tan, N.S., Sugii, S., Wong, M.T.C., Choong, C., 2017. Recellularization of decellularized adipose tissue-derived stem cells: role of the cell-secreted extracellular matrix in cellular differentiation. Biomater. Sci. 6, 168–178. https://doi.org/10.1039/c7bm00695k.

Hammond, M.A., Gallant, M.A., Burr, D.B., Wallace, J.M., 2014. Nanoscale changes in collagen are reflected in physical and mechanical properties of bone at the microscale in diabetic rats. Bone 60, 26–32. https://doi.org/10.1016/j.bone.2013.11.015.

Hankamolsiri, W., Manochantr, S., Tantrawatpan, C., Tantikanlayaporn, D., Tapanadechopone, P., Kheolamai, P., 2016. The effects of high glucose on

adipogenic and osteogenic differentiation of gestational tissue-derived MSCs. Stem Cells Int. 2016, 9674614. https://doi.org/10.1155/2016/9674614.
Hardouin, P., Rharass, T., Lucas, S., 2016. Bone marrow adipose tissue: to be or not to be a typical adipose tissue? Front. Endocrinol. 7, 85. https://doi.org/10.3389/fendo.2016.00085.
Hoshiba, T., Kawazoe, N., Tateishi, T., Chen, G., 2009. Development of stepwise osteogenesis-mimicking matrices for the regulation of mesenchymal stem cell functions [WWW document]. J. Biol. Chem. https://doi.org/10.1074/jbc.M109.054676.
Hoshiba, T., Kawazoe, N., Tateishi, T., Chen, G., 2010. Development of extracellular matrices mimicking stepwise adipogenesis of mesenchymal stem cells [WWW document]. Adv. Mater. Deerfield Beach Fla. https://doi.org/10.1002/adma.201000038.
Hoshiba, T., Kawazoe, N., Chen, G., 2012. The balance of osteogenic and adipogenic differentiation in human mesenchymal stem cells by matrices that mimic stepwise tissue development [WWW document]. Biomaterials. https://doi.org/10.1016/j.biomaterials.2011.11.061.
Hoshiba, T., Chen, G., Endo, C., Maruyama, H., Wakui, M., Nemoto, E., Kawazoe, N., Tanaka, M., 2016. Decellularized extracellular matrix as an in vitro model to study the comprehensive roles of the ECM in stem cell differentiation. Stem Cells Int. 2016 https://doi.org/10.1155/2016/6397820.
Hunt, H.B., Pearl, J.C., Diaz, D.R., King, K.B., Donnelly, E., 2018. Bone tissue collagen maturity and mineral content increase with sustained hyperglycemia in the KK-Ay murine model of type 2 diabetes. J. Bone Miner. Res. Off. J. Am. Soc. Bone Miner. Res. 33, 921–929. https://doi.org/10.1002/jbmr.3365.
Hunt, H.B., Miller, N.A., Hemmerling, K.J., Koga, M., Lopez, K.A., Taylor, E.A., Sellmeyer, D.E., Moseley, K.F., Donnelly, E., 2021. Bone tissue composition in postmenopausal women varies with glycemic control from normal glucose tolerance to type 2 diabetes mellitus. J. Bone Miner. Res. Off. J. Am. Soc. Bone Miner. Res. 36, 334–346. https://doi.org/10.1002/jbmr.4186.
Karim, L., Moulton, J., Van Vliet, M., Velie, K., Robbins, A., Malekipour, F., Abdeen, A., Ayres, D., Bouxsein, M.L., 2018. Bone microarchitecture, biomechanical properties, and advanced glycation end-products in the proximal femur of adults with type 2 diabetes. Bone 114, 32–39. https://doi.org/10.1016/j.bone.2018.05.030.
Karim, L., Rezaee, T., Vaidya, R., 2019. The effect of type 2 diabetes on bone biomechanics. Curr. Osteoporos. Rep. 17, 291–300. https://doi.org/10.1007/s11914-019-00526-w.
Keats, E., Khan, Z.A., 2012. Unique responses of stem cell-derived vascular endothelial and mesenchymal cells to high levels of glucose. PloS One 7, e38752. https://doi.org/10.1371/journal.pone.0038752.
Keats, E.C., Dominguez, J.M., Grant, M.B., Khan, Z.A., 2014. Switch from canonical to noncanonical wnt signaling mediates high glucose-induced adipogenesis. Stem Cells Dayt. Ohio 32, 1649–1660. https://doi.org/10.1002/stem.1659.
Lai, Y., Sun, Y., Skinner, C.M., Son, E.L., Lu, Z., Tuan, R.S., Jilka, R.L., Ling, J., Chen, X.-D., 2010. Reconstitution of marrow-derived extracellular matrix ex vivo: a robust culture system for expanding large-scale highly functional human mesenchymal stem cells. Stem Cells Dev. 19, 1095–1107. https://doi.org/10.1089/scd.2009.0217.
Lekkala, S., Taylor, E.A., Hunt, H.B., Donnelly, E., 2019. Effects of diabetes on bone material properties [WWW document]. Curr. Osteoporos. Rep. https://doi.org/10.1007/s11914-019-00538-6.
Li, M., Zhang, T., Jiang, J., Mao, Y., Zhang, A., Zhao, J., 2019. ECM coating modification generated by optimized decellularization process improves functional behavior of BMSCs. Mater. Sci. Eng. C Mater. Biol. Appl. 105, 110039 https://doi.org/10.1016/j.msec.2019.110039.
Lindner, U., Kramer, J., Behrends, J., Driller, B., Wendler, N.-O., Boehrnsen, F., Rohwedel, J., Schlenke, P., 2010. Improved proliferation and differentiation capacity of human mesenchymal stromal cells cultured with basement-membrane extracellular matrix proteins. Cytotherapy 12, 992–1005. https://doi.org/10.3109/14653249.2010.510503.
Mainreck, N., Brézillon, S., Sockalingum, Gd., Maquart, F.X., Manfait, M., Wegrowski, Y., 2011. Rapid characterization of glycosaminoglycans using a combined approach by infrared and Raman microspectroscopies [WWW document]. J. Pharm. Sci. https://doi.org/10.1002/jps.22288.
Mandair, G.S., Akhter, M.P., Esmonde-White, F.W.L., Lappe, J.M., Bare, S.P., Lloyd, W.R., Long, J.P., Lopez, J., Kozloff, K.M., Recker, R.R., Morris, M.D., 2021. Altered collagen chemical compositional structure in osteopenic women with past fractures: a case-control raman spectroscopic study. Bone 148, 115962. https://doi.org/10.1016/j.bone.2021.115962.
Marin, C., Papantonakis, G., Sels, K., van Lenthe, G.H., Falgayrac, G., Vangoitsenhoven, R., Van der Schueren, B., Penel, G., Luyten, F., Vandamme, K., Kerckhofs, G., 2018. Unraveling the compromised biomechanical performance of type 2 diabetes- and roux-en-Y gastric bypass bone by linking mechanical-structural and physico-chemical properties. Sci. Rep. 8, 5881. https://doi.org/10.1038/s41598-018-24229-x.
McManus, L.L., Burke, G.A., McCafferty, M.M., O'Hare, P., Modreanu, M., Boyd, A.R., Meenan, B.J., 2011. Raman spectroscopic monitoring of the osteogenic differentiation of human mesenchymal stem cells. Analyst 136, 2471–2481. https://doi.org/10.1039/c1an15167c.
Mendibil, U., Ruiz-Hernandez, R., Retegi-Carrion, S., Garcia-Urquia, N., Olalde-Graells, B., Abarrategi, A., 2020. Tissue-specific decellularization methods: rationale and strategies to achieve regenerative compounds [WWW document]. Int. J. Mol. Sci. https://doi.org/10.3390/ijms21155447.
Mieczkowska, A., Millar, P., Chappard, D., Gault, V.A., Mabilleau, G., 2020. Dapagliflozin and liraglutide therapies rapidly enhanced bone material properties and matrix biomechanics at bone formation site in a type 2 diabetic mouse model. Calcif. Tissue Int. 107, 281–293. https://doi.org/10.1007/s00223-020-00720-4.
Morandi, E.M., Verstappen, R., Zwierzina, M.E., Geley, S., Pierer, G., Ploner, C., 2016. ITGAV and ITGA5 diversely regulate proliferation and adipogenic differentiation of human adipose derived stem cells. Sci. Rep. 6, 1–14. https://doi.org/10.1038/srep28889.
Moseley, K.F., Du, Z., Sacher, S.E., Ferguson, V.L., Donnelly, E., 2021. Advanced glycation endproducts and bone quality: practical implications for people with type 2 diabetes. Curr. Opin. Endocrinol. Diabetes Obes. 28, 360–370. https://doi.org/10.1097/MED.0000000000000641.
Paschalis, E.P., Shane, E., Lyritis, G., Skarantavos, G., Mendelsohn, R., Boskey, A.L., 2004. Bone fragility and collagen cross-links [WWW document]. J. Bone Miner. Res. Off. J. Am. Soc. Bone Miner. Res. https://doi.org/10.1359/JBMR.040820.
Penel, G., Leroy, G., Rey, C., Bres, E., 1998. MicroRaman spectral study of the PO4 and CO3 vibrational modes in synthetic and biological apatites. Calcif. Tissue Int. 63, 475–481. https://doi.org/10.1007/s002239900561.
Pezzotti, G., Rondinella, A., Marin, E., Zhu, W., Nn, A., Ulian, G., Valdrè, G., 2017. Raman spectroscopic investigation on the molecular structure of apatite and collagen in osteoporotic cortical bone [WWW document]. J. Mech. Behav. Biomed. Mater. https://doi.org/10.1016/j.jmbbm.2016.08.030.
Rharass, T., Lucas, S., 2018. MECHANISMS IN ENDOCRINOLOGY: bone marrow adiposity and bone, a bad romance? Eur. J. Endocrinol. https://doi.org/10.1530/EJE-18-0182.
Rharass, T., Lucas, S., 2019. High glucose level impairs human mature bone marrow adipocyte function through increased ROS production. Front. Endocrinol. 10, 607. https://doi.org/10.3389/fendo.2019.00607.
Rokidi, S., Paschalis, E.P., Klaushofer, K., Vennin, S., Desyatova, A., Turner, J.A., Watson, P., Lappe, J., Akhter, M.P., Recker, R.R., 2019. Organic matrix quality discriminates between age- and BMD-matched fracturing versus non-fracturing post-menopausal women: a pilot study [WWW document]. Bone. https://doi.org/10.1016/j.bone.2019.06.017.
Rossi, E., Guerrero, J., Aprile, P., Tocchio, A., Kappos, E.A., Gerges, I., Lenardi, C., Martin, I., Scherberich, A., 2018. Decoration of RGD-mimetic porous scaffolds with engineered and devitalized extracellular matrix for adipose tissue regeneration. Acta Biomater. 73, 154–166. https://doi.org/10.1016/j.actbio.2018.04.039.
Rupani, A., Hidalgo-Bastida, L.A., Rutten, F., Dent, A., Turner, I., Cartmell, S., 2012. Osteoblast activity on carbonated hydroxyapatite [WWW document]. J. Biomed. Mater. Res. A. https://doi.org/10.1002/jbm.a.34037.
Sabater, D., Arriarán, S., Romero, M.del M., Agnelli, S., Remesar, X., Fernández-López, J. A., Alemany, M., 2014. Cultured 3T3L1 adipocytes dispose of excess medium glucose as lactate under abundant oxygen availability. Sci. Rep. 4, 1–9. https://doi.org/10.1038/srep03663.
Sadie-Van Gijsen, H., Crowther, N.J., Hough, F.S., Ferris, W.F., 2013. The interrelationship between bone and fat: from cellular see-saw to endocrine reciprocity. Cell. Mol. Life Sci. CMLS 70, 2331–2349. https://doi.org/10.1007/s00018-012-1211-2.
Saito, M., Fujii, K., Mori, Y., Marumo, K., 2006. Role of collagen enzymatic and glycation induced cross-links as a determinant of bone quality in spontaneously diabetic WBN/Kob rats. Osteoporos. Int. J. Establ. Result Coop. Eur. Found. Osteoporos. Natl. Osteoporos. Found. USA 17, 1514–1523. https://doi.org/10.1007/s00198-006-0155-5.
Schäck, L.M., Noack, S., Winkler, R., Wißmann, G., Behrens, P., Wellmann, M., Jagodzinski, M., Krettek, C., Hoffmann, A., 2013. The phosphate source influences gene expression and quality of mineralization during in vitro osteogenic differentiation of human mesenchymal stem cells. PLOS ONE 8, e65943. https://doi.org/10.1371/journal.pone.0065943.
Schlesinger, P.H., Blair, H.C., Beer Stolz, D., Riazanski, V., Ray, E.C., Tourkova, I.L., Nelson, D.J., 2019. Cellular and extracellular matrix of bone, with principles of synthesis and dependency of mineral deposition on cell membrane transport. Am. J. Phys. Cell Physiol. 318, C111–C124. https://doi.org/10.1152/ajpcell.00120.2019.
Schwartz, A.V., 2016. Epidemiology of fractures in type 2 diabetes. Bone 82, 2–8. https://doi.org/10.1016/j.bone.2015.05.032.
Shao, X., Cao, X., Song, G., Zhao, Y., Shi, B., 2014. Metformin rescues the MG63 osteoblasts against the effect of high glucose on proliferation. J. Diabetes Res. 2014, 453940 https://doi.org/10.1155/2014/453940.
Shi, P., Hou, A., Li, C., Wu, X., Jia, S., Cen, H., Hu, X., Gong, H., 2021. Continuous subcutaneous insulin infusion ameliorates bone structures and mechanical properties in type 2 diabetic rats by regulating bone remodeling. Bone 153, 116101. https://doi.org/10.1016/j.bone.2021.116101.
Suchacki, K.J., Tavares, A.A.S., Mattiucci, D., Scheller, E.L., Papanastasiou, G., Gray, C., Sinton, M.C., Ramage, L.E., McDougald, W.A., Lovdel, A., Sulston, R.J., Thomas, B. J., Nicholson, B.M., Drake, A.J., Alcaide-Corral, C.J., Said, D., Poloni, A., Cinti, S., Macpherson, G.J., Dweck, M.R., Andrews, J.P.M., Williams, M.C., Wallace, R.J., van Beek, E.J.R., MacDougald, O.A., Morton, N.M., Stimson, R.H., Cawthorn, W.P., 2020. Bone marrow adipose tissue is a unique adipose subtype with distinct roles in glucose homeostasis. Nat. Commun. 11, 3097. https://doi.org/10.1038/s41467-020-16878-2.
Sun, Y., Li, W., Lu, Z., Chen, R., Ling, J., Ran, Q., Jilka, R.L., Chen, X.-D., 2011. Rescuing replication and osteogenesis of aged mesenchymal stem cells by exposure to a young extracellular matrix. FASEB J. 25, 1474–1485. https://doi.org/10.1096/fj.10-161497.
Tencerova, M., Ferencakova, M., Kassem, M., 2021. Bone marrow adipose tissue: role in bone remodeling and energy metabolism. Best Pract. Res. Clin. Endocrinol. Metab. https://doi.org/10.1016/j.beem.2021.101545.
Tice, M.J.L., Bailey, S., Sroga, G.E., Gallagher, E.J., Vashishth, D., 2021. Non-obese MKR mouse model of type 2 diabetes reveals skeletal alterations in mineralization and material properties [WWW document]. JBMR Plus. https://doi.org/10.1002/jbm4.10583.

Unal, M., Creecy, A., Nyman, J.S., 2018. The role of matrix composition in the mechanical behavior of bone. Curr. Osteoporos. Rep. 16, 205–215. https://doi.org/10.1007/s11914-018-0433-0.

Viguet-Carrin, S., Garnero, P., Delmas, P.D., 2006. The role of collagen in bone strength [WWW document]. Osteoporos. Int. J. Establ. Result Coop. Eur. Found. Osteoporos. Natl. Osteoporos. Found. USA. https://doi.org/10.1007/s00198-005-2035-9.

Wang, W., Zhang, X., Zheng, J., Yang, J., 2010. High glucose stimulates adipogenic and inhibits osteogenic differentiation in MG-63 cells through cAMP/protein kinase A/extracellular signal-regulated kinase pathway. Mol. Cell. Biochem. 338, 115–122. https://doi.org/10.1007/s11010-009-0344-6.

Wang, L., Johnson, J.A., Zhang, Q., Beahm, E.K., 2013. Combining decellularized human adipose tissue extracellular matrix and adipose-derived stem cells for adipose tissue engineering [WWW document]. Acta Biomater. https://doi.org/10.1016/j.actbio.2013.06.035.

Wang, A., Midura, R.J., Vasanji, A., Wang, A.J., Hascall, V.C., 2014. Hyperglycemia diverts dividing osteoblastic precursor cells to an adipogenic pathway and induces synthesis of a hyaluronan matrix that is adhesive for monocytes. J. Biol. Chem. 289, 11410–11420. https://doi.org/10.1074/jbc.M113.541458.

Wang, L., Zhang, H., Wang, S., Chen, X., Su, J., 2021. Bone marrow adipocytes: a critical player in the bone marrow microenvironment. Front. Cell Dev. Biol. 9, 770705 https://doi.org/10.3389/fcell.2021.770705.

Wen, X.X., Wang, F.Q., C, X., Wu, Z.X., Zhang, Y., Feng, Y.F., Yan, Y.B., Lei, W., 2015. Time related changes of mineral and collagen and their roles in cortical bone mechanics of ovariectomized rabbits [WWW document]. PloS One. https://doi.org/10.1371/journal.pone.0127973.

Yerramshetty, J.S., Lind, C., Akkus, O., 2006. The compositional and physicochemical homogeneity of male femoral cortex increases after the sixth decade [WWW document]. Bone. https://doi.org/10.1016/j.bone.2006.06.002.

Yu, E.W., Greenblatt, L., Eajazi, A., Torriani, M., Bredella, M.A., 2017. Marrow adipose tissue composition in adults with morbid obesity. Bone 97, 38–42. https://doi.org/10.1016/j.bone.2016.12.018.

Zhang, Y., Yang, J.-H., 2013. Activation of the PI3K/Akt pathway by oxidative stress mediates high glucose-induced increase of adipogenic differentiation in primary rat osteoblasts. J. Cell. Biochem. 114, 2595–2602. https://doi.org/10.1002/jcb.24607.